STRUCTURED-INITIALIZATION LEARNING

Anonymous authors
Paper under double-blind review

ABSTRACT

The emergence of large language models (LLMs) has revolutionized natural language processing, but their development and deployment face significant challenges in computational resources and environmental sustainability. Traditional self-supervised learning (SSL) paradigms requiring extensive computational infrastructure and exhibiting slow convergence rates, leading to increased energy consumption and longer training durations. While existing model fine-tuning techniques such as Low-Rank Adaptation (LoRA) are resource-intensive and fail to facilitate swift knowledge updates when integrating a mount of new data in model version iteration. To mitigate these challenges, we introduce **S**tructured-initi**a**l**i**zation **l**earning (SAIL), a novel method for accelerating the training of neural network models by leveraging knowledge from (publicly available) pre-trained models. Our approach comprises two key components: (1) a parameter transformation technique that adjusts the dimensions of pre-trained model parameters to match the target architecture, and (2) a proximal parameter integration and retraining strategy that efficiently combines transformed parameters to initialize new models. We formalize the concept of Proximal Parameter and provide theoretical guarantees for its convergence advantages. Our approach achieves substantial reductions in training time and computational resources while maintaining or improving model performance on downstream tasks. These results indicate that SAIL provides a promising direction for the more efficient and accessible development of the deep learning community. Our code will be made publicly available.

1 INTRODUCTION

The emergence of Large Language Models (LLMs) such as GPT-3 (Brown et al., 2020), GPT-4 (OpenAI et al., 2023), PaLM (Chowdhery et al., 2023), and Gemini (Team et al., 2023) has ushered in a new era of natural language processing. These models have demonstrated unprecedented capabilities across a wide range of sequence tasks, showcasing remarkable advancements in representation learning. However, their success is accompanied by significant challenges. The development and deployment of LLMs require enormous computational resources, raising serious concerns about environmental sustainability and accessibility (Strubell et al., 2020). Moreover, while recent advancements have introduced efficient methods for data augmentation (Zhou et al., 2024) and synthesis of higher-quality data (Kaddour et al., 2023) to streamline the dataset, the pre-training process for these models remains prohibitively expensive and time-consuming (Sun et al., 2017).

A similar challenge constrains the advancement of self-supervised learning in both language and vision domains. Specifically, self-supervised learning for large models effectively leverages unlabeled data for representation learning (Liu, 2019; He et al., 2020; Chen et al., 2020), but it faces significant challenges in convergence speed and efficiency (Liu & Zhao, 2021; Wang et al., 2021). This paradigm renders the learning and fine-tuning process particularly resource-intensive (Faiz et al., 2023; Gao et al., 2020). As diverse new training data are curated, including high-quality synthetic data (Fan et al., 2024), the computational demands continue to escalate.

While techniques like LoRA and QLoRA (Hu et al., 2021; Dettmers et al., 2024; SONG et al., 2024) enable efficient fine-tuning of pre-trained models on domain-specific data, and model editing techniques (Meng et al., 2022) allow for rapid knowledge modification, these methods still demand substantial resources. Multiple modifications and edits can lead to model collapse (Wu & Papyan, 2024; Gu et al., 2024). Moreover, as indicated by Zhu & Li (2023), post-training fine-tuning struggles to rectify erroneous knowledge learned during the training phase, potentially perpetuating hallucina-

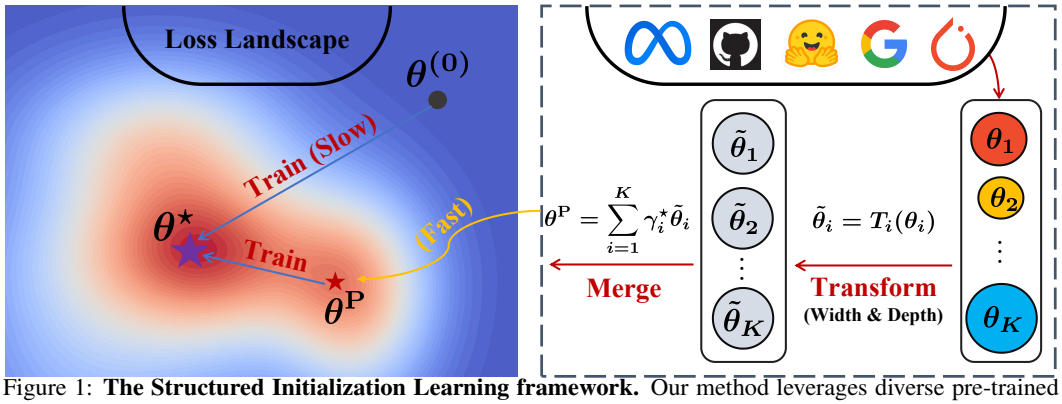

Figure 1: **The Structured Initialization Learning framework.** Our method leverages diverse pre-trained models from open-source platforms, applying weight linear transformations to adapt them to the target model size. We then merge these transformed models through parameter aggregation, creating a informative initialization ($\boldsymbol{\theta}^{\mathrm{P}}$). This amalgamated starting point serves as the initial parameters in the Loss Space, enabling a more efficient optimization trajectory towards the optimal parameters ($\boldsymbol{\theta}^{\star}$) for the new target model. This unified framework can facilitate rapid model iteration on new datasets while harnessing the advantages of pre-trained models, leading to faster convergence to the $\boldsymbol{\theta}^{\star}$.

tions (Ji et al., 2023) and persistent model biases (Blodgett et al., 2020). Furthermore, fine-tuning is typically infeasible when dealing with changes to model architecture (Dettmers et al., 2024). Consequently, the current strategy for updating model versions with architectural, capacity, and knowledge modifications——such as progressing from Llama 1 to Llama 2/3 (Touvron et al., 2023)——involves training new models from scratch using large volumes of fresh data through repeated training cycles.

Building upon the preceding analysis, we propose that a key computational challenge in current model training methods lies in their failure to effectively leverage knowledge from cross-architectural and cross-domain pre-trained models, instead relying solely on training from randomly initialized models. The question then arises: *how can we effectively utilize pre-trained models to initially tap into their existing knowledge, followed by efficient new training or continued training?*

In this paper, we aim to harness pre-trained models to obtain an initialized parameter that is proximal to optimal parameter of model that accelerates the training of a new large model, facilitating easier adaptation to new data and techniques. To achieve this, we first need to transform the parameters of previously trained models to match the parameter size and architecture of our new target model. We then need to find an optimal integration of these parameters to form the proximal parameter.

To address these challenges and bridge the gap, we introduce an innovative training paradigm:

Proposition 1 (Accelerating task-agnostic training via pre-trained model knowledge) . *Let $M = \{\psi_1, \ldots, \psi_k, \psi_K\}$ be a set of models pre-trained over datasets $S = \{D_1, \ldots, D_K\}$, D a new dataset, $\phi_{\boldsymbol{\theta}^{(0)}}$ a initialized model, and $\mathscr{L}_D$ a training process with T steps on data D. We propose a parameter initializer $\mathscr{P}$ centered on $\boldsymbol{\theta}$, aimed at improving training efficiency such that:*

$$\mathcal{L}_D(\boldsymbol{\theta}^{(T)} \leftarrow \mathscr{L}_D(\boldsymbol{\theta}^{(0)} \leftarrow \mathscr{P}(M, S))) < \mathcal{L}_D(\boldsymbol{\theta}^{(T)} \leftarrow \mathscr{L}_D(\boldsymbol{\theta}^{(0)}))\,, \tag{1}$$

where $\mathcal{L}_D$ represents the loss function evaluating performance on data D.

To investigate our new learning paradigm claim in Proposition 1 , we introduce SAIL, a novel method that leverages freely available pre-trained models to accelerate training. Our approach improves efficiency in the initial training stages by effectively utilizing the parameters of pre-trained models directly, thus establishing a rapid pathway for representation model training (see Figure 1).

The core of our method involves inheriting and integrating knowledge directly from pre-trained model parameters, creating a shortcut in the learning process. This approach allows the initial model ϕ to effectively reach a "Proximal Parameter" $\boldsymbol{\theta}^{\mathrm{P}}$ that is closer to optimal than randomly initialized parameters, thereby significantly accelerating the learning process. As formalized in Definition 1 , our method first aligns the parameter dimensions from various pre-trained models into a unified format. Subsequently, we execute a weighted parameter averaging that accounts for the effective knowledge embedded in the parameters of each model, thereby enhancing both knowledge transfer and representation learning efficiency.

This framework leverages the extensive range of publicly available pre-trained models, providing a novel paradigm for representation learning and notably expediting the model development process. Our main contributions are as follows:

(a) We introduce SAIL, a novel method for accelerating the training of large language models by leveraging knowledge from pre-trained models. This approach includes a parameter transformation technique and a proximal parameter integration strategy, effectively utilizing the wealth of publicly available models (see Section 4).
(b) We provide theoretical foundations for our method, including the formalization of the Proximal Parameter concept and convergence guarantees. Our analysis demonstrates how SAIL leads to faster convergence compared to random initialization (see Section 3 and Appendix A).
(c) We conduct extensive experiments across multiple modalities, including natural language processing and computer vision tasks and various model architectures. Our results show that SAIL not only accelerates training on its own but also demonstrates consistent performance improvements across different datasets, model sizes, and learning paradigms (supervised and self-supervised). This versatility is evidenced by experiments on GPT-2 variants for NLP and ResNet architectures for image classification, showcasing the broad applicability of our method. (see Section 4.4 and Section 4.5).

2 Related Work

Our work on SAIL builds upon and extends several areas of research in efficient training techniques, particularly for LLMs. We discuss three distinct relevant areas: 1) techniques for efficient training; 2) methods for transforming and reusing deep models; and 3) model merging methods to combine different models.

Efficient training techniques for representation learning. A critical aspect of efficient training involves effective model initialization, which can significantly influence convergence speed and overall training efficiency. Techniques such as Xavier Initialization (Glorot & Bengio, 2010) and Kaiming Initialization (He et al., 2015) have been foundational in ensuring stable gradients and accelerating convergence during training.

Beyond initialization, dynamic architecture approaches achieve efficiency by dynamically activating or deactivating network components during training, employing strategies such as layer stacking (Gong et al., 2019), layer dropping (Zhang & He, 2020), and the use of sparse attention mechanisms (Child et al., 2019). Batch selection techniques enhance learning efficiency by prioritizing the most informative training examples, utilizing methods like selective backprop (Jiang et al., 2019), RHO loss (Mindermann et al., 2022), and curriculum learning (Bengio et al., 2009). Furthermore, innovative optimizers such as Lion (Wang et al., 2023a), Sophia (Liu et al., 2023), and AdaFactor (Shazeer & Stern, 2018) provide alternatives to traditional optimizers like Adam(W), promoting more efficient convergence. Techniques like mixed-precision training (Micikevicius et al., 2017) and gradient checkpointing (Chen et al., 2016) further mitigate computational demands by reducing memory consumption, thereby enabling the training of larger models on limited hardware resources.

Unlike these methods, our SAIL directly leverages the parameters of multiple pre-trained models to create a well-informed starting point, potentially reducing the need for complex training optimizations. While these existing techniques could be combined with our approach for further efficiency gains.

Model reuse and expansion. Approaches in this category focus on leveraging pre-existing knowledge to initialize or expand models. Model reuse methods enable the adaptation of pre-trained models for new tasks or larger architectures without retraining from scratch. Notable examples include Samragh et al. (2024), who explore scalable model reuse strategies, and Wang et al. (2023b), who investigate data-driven approaches for model adaptation.

Model expansion techniques aim to scale smaller models to initialize larger ones, ensuring that the expanded models retain the learned representations. Classic methods like Net2Net (Chen et al., 2015) provide a foundation for expanding neural networks by transferring knowledge from smaller to larger architectures. More recent advancements, such as Learning to Grow (Wang et al., 2023a) and MorphNet (Gordon et al., 2018), focus on dynamically increasing model capacity during training, thereby enhancing scalability and performance.

Progressive learning methods gradually increase model capacity during training, which can lead to more efficient learning and better generalization. Works by Li et al. (2022); Pan et al. (2024) introduce automated strategies for progressive model scaling.

Knowledge transfer techniques utilize distillation to transfer knowledge from smaller to larger models or between models of similar sizes, enhancing performance and training efficiency. Methods such as Knowledge Inheritance (Qin et al., 2021) and Born-Again Networks (Furlanello et al., 2018) exemplify effective strategies for transferring learned representations.

Our research focuses on the novel capability to incorporate parameters from multiple pre-trained models with diverse architectures. This approach generates a sophisticated initialization for the target model, surpassing conventional methods that are limited to single-model adaptation or expansion.

Model merging. This area focuses on combining multiple models to create a single, more powerful model. Simple approaches like Model Soup (Wortsman et al., 2022) apply straightforward weight averaging to merge models, thus combining their diverse learned representations. Advancements such as Checkpoint Merging (Liu et al., 2024) introduce Bayesian optimization to effectively select and weight various checkpoints, resulting in a more robust and high-performing merged model. Additionally, techniques like cross-model integration via MindMerger (Huang et al., 2024) enable the fusion of models with varying specializations, enhancing the overall capabilities of the merged system. Dynamic expert merging methods, including DELLA-Merging (Tej Deep et al., 2024), integrate specialized expert models dynamically, allowing the merged model to adapt to a variety of tasks during inference. Adaptive weighting approaches such as AdaMerging (Yang et al., 2023) and MetaGPT (Zhou et al., 2024) leverage dynamic weighting schemes and meta-learning to fine-tune the merging process, ensuring optimal integration of constituent models' strengths. Furthermore, task-oriented merging strategies like Task Arithmetic (Ilharco et al., 2022), Language and Task Arithmetic (Chronopoulou et al., 2023), and Task Arithmetic in Tangent Space (Ortiz-Jimenez et al., 2024) focus on blending models trained on different tasks, thereby creating versatile LLMs adept at multiple applications.

3 Accelerated Training via Proximal Parameter

In this section, we formalize the problem of accelerating the training of large auto-regressive language models (LLMs) by leveraging knowledge from pre-trained models. We introduce the concept of *Proximal Parameter*, which serves as the foundation for our acceleration technique. We present rigorous mathematical definitions and theorems illustrating the accelerated convergence benefits of using proximal parameter initialization for model training.

3.1 Proximal Parameter

Let $\boldsymbol{\phi}_{\boldsymbol{\theta}} : \mathcal{X} \to \mathcal{Y}$ denote an model parameterized by $\boldsymbol{\theta} \in \mathbb{R}^d$, where $\mathcal{X}$ is the input space and $\mathcal{Y}$ is the output space. Let $\ell : \mathcal{Y} \times \mathcal{Y} \to \mathbb{R}_{\geq 0}$ be a loss function measuring the discrepancy between the output of model and the target output. Our goal is to minimize the expected loss $\mathbb{E}\left[\ell(\boldsymbol{\phi}_{\boldsymbol{\theta}}(\mathbf{x}), \mathbf{y})\right]$:

$$\boldsymbol{\theta}^\star = \arg\min_{\boldsymbol{\theta}} \{\mathcal{J}_D(\boldsymbol{\theta})\} = \arg\min_{\boldsymbol{\theta}} \{\mathbb{E}_{(\mathbf{x},\mathbf{y})\sim D}\left[\ell(\boldsymbol{\phi}_{\boldsymbol{\theta}}(\mathbf{x}), \mathbf{y})\right]\}, \tag{2}$$

where $(\mathbf{x}, \mathbf{y})$ are input-output pairs sampled from real data distribution D and $\mathbf{y} \in \mathcal{Y}$.

To accelerate convergence during training, we aim to find an effective initialization for the model parameters $\boldsymbol{\theta}$. The key insight is that we can leverage the knowledge encoded in multiple pre-trained models to construct a more informed starting point for training the new model. We now introduce the concept of *Proximal Parameter*, which represents an aggregation of knowledge from multiple pre-trained models, adjusted to match the architecture and knowledge of the target model $\boldsymbol{\phi}_{\boldsymbol{\theta}^\star}$.

Definition 1 (Proximal Parameter). *Let $\{\boldsymbol{\theta}_1, \boldsymbol{\theta}_2, \ldots, \boldsymbol{\theta}_K\}$ be a set of K parameter vectors from pre-trained models M, where each $\boldsymbol{\theta}_i \in \mathbb{R}^{d_i}$. Define $\boldsymbol{T}_i : \mathbb{R}^{d_i} \to \mathbb{R}^d$ as a transformation function mapping each $\boldsymbol{\theta}_i$ to the parameter space $\mathbb{R}^d$ of the target model $\boldsymbol{\phi}_{\boldsymbol{\theta}^\star}$. The proximal parameter $\boldsymbol{\theta}^{\mathrm{P}} \in \mathbb{R}^d$ is the optimal linear combination of the transformed parameters, weighted by γ_i, defined*

as $\boldsymbol{\theta}^{\mathrm{P}} = \sum_{i=1}^{K} \gamma_i^\star \tilde{\boldsymbol{\theta}}_i$ *based on the loss function* $\mathcal{J}_D$ *and training process* $\mathscr{L}_D$ *such that:*

$$\gamma_1^\star, \ldots, \gamma_K^\star = \arg\min_{\gamma_1,\ldots,\gamma_K} \{\mathcal{J}_D(\mathscr{L}_D(\textstyle\sum_{i=1}^{K} \gamma_i \tilde{\boldsymbol{\theta}}_i))\}. \tag{3}$$

However, calculating (3) poses a challenge due to the nonlinear properties of $\mathcal{J}_D$ *and* $\mathscr{L}_D$*. Alternatively, define the proximal parameter based on Frobenius norm in parameter space as:*

$$\gamma_1^\star, \ldots, \gamma_K^\star = \arg\min_{\gamma_1,\ldots,\gamma_K} \left\| \textstyle\sum_{i=1}^{K} \gamma_i \tilde{\boldsymbol{\theta}}_i - \boldsymbol{\theta}^\star \right\|_F^2, \tag{4}$$

where the transformed parameters are defined as $\tilde{\boldsymbol{\theta}}_i = \boldsymbol{T}_i(\boldsymbol{\theta}_i) \in \mathbb{R}^d$ *for* $i = 1, \ldots, K$.

The proximal parameter $\boldsymbol{\theta}^{\mathrm{P}}$ aggregates information from multiple pre-trained models into a single set of parameters, serving as an informed initialization for the target model.

3.2 Convergence Analysis

Before presenting the theorem, we introduce key assumptions that underpin our analysis. We concentrate on linear models, assuming that all pre-trained models share an identical architecture. Under these conditions, any variation among the models stems solely from differences in their training datasets. Additionally, in linear models, the parameters are uniquely determined by the training data. These assumptions allow us to quantify model proximity by examining dataset differences, offering a coherent framework for comparing pre-trained models with randomly initialized ones.

Theorem 1 (Proximity-based model initialization advantage, ***proof in Appendix A*** **).** *For any proportionality factor* $\alpha \in (0, 1)$*, the squared Euclidean distance between the pre-trained model parameters* $\boldsymbol{\theta}_i$ *and the target parameters* $\boldsymbol{\theta}^\star$ *satisfies the following probabilistic bound:*

$$\Pr\left(\|\boldsymbol{\theta}_i - \boldsymbol{\theta}^\star\|_2^2 \leq \alpha \|\boldsymbol{\theta}_{rand} - \boldsymbol{\theta}^\star\|_2^2\right) \geq 1 - O\left(\tfrac{\tau^2+\beta}{\alpha}\right), \tag{5}$$

Here, $\boldsymbol{\theta}_{rand}$ *represents the randomly initialized model parameters,* τ *quantifies the variance of the pre-training dataset mean difference compared to the target dataset, while* β *represents the upper bound on the variance of the perturbation in the pre-training dataset's variance. Smaller values of* τ *and* β *reflect greater proximity between* $\boldsymbol{\theta}_i$ *and* $\boldsymbol{\theta}^\star$*.*

Theorem 1 shows that, with high probability, pre-trained parameters $\boldsymbol{\theta}_i$ are closer to the optimal target parameters $\boldsymbol{\theta}^\star$ than randomly initialized parameters, especially when the pre-training dataset distribution D_i is statistically similar to the target $D^\star$.

Theorem 2 (Convergence of proximal parameter initialization, ***proof in Appendix B*** **).** *Let* $\{\boldsymbol{\theta}^{(t)}\}$ *be the sequence of parameters generated by gradient descent with fixed learning rate* $\eta \in \left(0, \frac{1}{L}\right)$*, initialized at* $\boldsymbol{\theta}^{(0)} = \boldsymbol{\theta}^P = \sum_{i=1}^{n} \gamma_i^\star \tilde{\boldsymbol{\theta}}_i$*, where* $\boldsymbol{\theta}^P$ *is defined as in (3). Then, the suboptimality at iteration* T *satisfies:*

$$\mathcal{J}_D(\boldsymbol{\theta}^{(T)}) - \mathcal{J}_D(\boldsymbol{\theta}^\star) \leq (1 - \eta\mu)^T \left(\mathcal{J}_D(\boldsymbol{\theta}^P) - \mathcal{J}_D(\boldsymbol{\theta}^\star)\right), \tag{6}$$

where $L > 0$ *is the Lipschitz constant of the gradient of the loss function* $\mathcal{J}_D(\boldsymbol{\theta})$*, and* $\mu > 0$ *is the strong convexity parameter of* $\mathcal{J}_D(\boldsymbol{\theta})$*. Furthermore, we have:*

$$\mathcal{J}_D(\boldsymbol{\theta}^P) - \mathcal{J}_D(\boldsymbol{\theta}^\star) \leq \tfrac{L}{2} \left\|\boldsymbol{\theta}^P - \boldsymbol{\theta}^\star\right\|_2^2. \tag{7}$$

By choosing the weights $\gamma_i^\star$ *to minimize* $\left\|\boldsymbol{\theta}^P - \boldsymbol{\theta}^\star\right\|_2$*, we effectively minimize the bound on the initial suboptimality, leading to faster convergence compared to random initialization.*

In light of Theorem 2, we propose that initializing with the proximal parameter $\boldsymbol{\theta}^P$ is likely to lead to faster convergence compared to random initialization. Specifically, Theorem 2 shows that the convergence rate of the loss function can be controlled by the initial parameter distance, while Theorem 1 demonstrates that the distance between the proximal parameter $\boldsymbol{\theta}^P$ and the

optimal parameter $\boldsymbol{\theta}^\star$ is, with high probability, smaller than that of randomly initialized parameters. Therefore, by combining these results, we can assert that, with high probability, initialization with the proximal parameter $\boldsymbol{\theta}^P$ leads to faster convergence compared to random initialization. A detailed proof of this argument can be found in Appendix C. Moreover, by weighting the contributions of each transformed parameter, we can prioritize models closer to the target. This strategy ensures that the optimization process starts from a point nearer to the global optimum, thereby enhancing the overall convergence rate of the gradient descent algorithm.

4 STRUCTURED-INITIALIZATION LEARNING

In this section, we introduce SAIL, a novel approach that accelerates the training of large language models by directly leveraging the parameters of pre-trained models. Traditional methods, such as knowledge distillation, focus on aligning model outputs or hidden states, often neglecting the rich information embedded in the model parameters themselves. We posit that the parameters of a model encapsulate compressed knowledge acquired during training, and different models may provide diverse perspectives even when trained on similar data. By directly utilizing these parameters, we aim to create an effective starting point for training new models, leading to faster convergence and improved performance.

Our methodology comprises two main components: (1) *Parameter Transformation*, where we adjust the dimensions of pre-trained model parameters to match the target model architecture, and (2) *Proximal Parameter Integration and Retraining*, where we integrate the transformed parameters to initialize the new model and continue training on new data.

4.1 PARAMETER TRANSFORMATION

To harness the knowledge embedded in pre-trained models, we first transform their parameters to be compatible with the target model's architecture. This involves adjusting both the *width* (dimensionality of layers) and the *depth* (number of layers) of the models.

Width transformation. For each layer in the model, we define a *width transformation* function that maps the parameters from the source dimensionality to the target dimensionality. Given a weight matrix $\boldsymbol{\theta} \in \mathbb{R}^{d_{\text{in}} \times d_{\text{out}}}$ from a pre-trained model, we aim to transform it into a matrix $\tilde{\boldsymbol{\theta}} \in \mathbb{R}^{d'_{\text{in}} \times d'_{\text{out}}}$ that aligns with the target model's dimensions.

$$\tilde{\boldsymbol{\theta}} = \begin{bmatrix} \mathbf{c}_{11} & \mathbf{c}_{12} & \cdots & \mathbf{c}_{1d_{\text{in}}} \\ \mathbf{c}_{21} & \mathbf{c}_{22} & \cdots & \mathbf{c}_{2d_{\text{in}}} \\ \vdots & \vdots & \ddots & \vdots \\ \mathbf{c}_{d'_{\text{in}}1} & \mathbf{c}_{d'_{\text{in}}2} & \cdots & \mathbf{c}_{d'_{\text{in}}d_{\text{in}}} \end{bmatrix} \mathbf{D} \begin{bmatrix} \mathbf{c}'_{11} & \mathbf{c}'_{12} & \cdots & c'_{1d'_{\text{out}}} \\ \mathbf{c}'_{21} & \mathbf{c}'_{22} & \cdots & c'_{2d'_{\text{out}}} \\ \vdots & \vdots & \ddots & \vdots \\ \mathbf{c}'_{d_{\text{out}}1} & \mathbf{c}'_{d_{\text{out}}2} & \cdots & \mathbf{c}'_{d_{\text{out}}d'_{\text{out}}} \end{bmatrix}^\top \tag{8}$$

where $\mathbf{c}_{\text{in}} \in \mathbb{R}^{d'_{\text{in}} \times d_{\text{in}}}$ and $\mathbf{c}_{\text{out}} \in \mathbb{R}^{d'_{\text{out}} \times d_{\text{out}}}$ are transformation matrices that map dimensions from the source to the target. This mapping can be learned or defined using schemes such as random projection or interpolation, followed by normalization to ensure numerical stability.

Depth transformation. To adjust the number of layers, we introduce a *depth transformation* function that combines or splits the parameters of layers. Given L layers in the pre-trained model and L' layers in the target model, we define:

$$\tilde{\boldsymbol{\theta}}^k = \begin{bmatrix} d_{k1} & d_{k2} & \cdots & d_{kL} \end{bmatrix} \begin{bmatrix} \boldsymbol{\theta}^1 \\ \boldsymbol{\theta}^2 \\ \vdots \\ \boldsymbol{\theta}^L \end{bmatrix}, \quad \text{for } k = 1, \ldots, L' \tag{9}$$

Here, $\tilde{\boldsymbol{\theta}}^k$ represents the parameters of the k-th layer in the target model. The transformation is defined as a linear combination of the source model's layer parameters $\boldsymbol{\theta}^i$ ($i = 1, \ldots, L$). The coefficient matrix $\mathbf{D}_{\text{depth}} = [d_{ki}] \in \mathbb{R}^{L' \times L}$ controls this linear combination. For each row k of $\mathbf{D}_{\text{depth}}$ corresponds to a layer in the target model. Each column i corresponds to a layer in the source model. The element d_{ki} represents the contribution of the i-th source layer to the k-th target layer.

4.2 Proximal Parameter Integration and Retraining

After transforming the parameters of the pre-trained models to match the target architecture, we integrate them to form the proximal parameter $\boldsymbol{\theta}^{\mathrm{P}}$ as defined in (3).

Integration of transformed parameters based on total variation distance. Using the transformed parameter $\tilde{\boldsymbol{\theta}}_i$, we compute the proximal parameter by *approximately optimal* weights $\gamma_i^\star$, i.e., $\boldsymbol{\theta}^{\mathrm{P}} = \sum_{i=1}^n \gamma_i^\star \tilde{\boldsymbol{\theta}}_i$. Specifically, let $\mathrm{D}_{\mathrm{TV}}(P, Q)$ denote the total variation distance between two distributions. Building on Theorem 3, we can compute the approximately optimal weights $\gamma_i^\star$.

Theorem 3 (Optimal combination coefficients, *proof in Appendix E*). *Given the proximal parameter $\boldsymbol{\theta}^{\mathrm{P}} \in \mathbb{R}^d$, defined as the weighted convex combination of transformed parameters:*

$$\boldsymbol{\theta}^{\mathrm{P}} = \textstyle\sum_{i=1}^n \gamma_i^\star \tilde{\boldsymbol{\theta}}_i, \quad \text{where} \quad \sum_{i=1}^n \gamma_i^\star = 1, \quad \gamma_i^\star \geq 0, \tag{10}$$

the optimal combination coefficients $\boldsymbol{\gamma}^\star = [\gamma_1^\star, \gamma_2^\star, \ldots, \gamma_n^*]^\top$ that minimize the distance between $\boldsymbol{\theta}^{\mathrm{P}}$ and the target parameter $\boldsymbol{\theta}^\star$ are as follows:

(a) ***Case** $n = 2$: When there are two pre-trained models, the optimal combination coefficients $\gamma_1^\star$ and $\gamma_2^\star$ can be explicitly determined under the constraint $\gamma_i^\star \geq 0$:*

$$\gamma_1^\star = \frac{\mathrm{D}_{TV}(D_2, D^\star)^2 + \mathrm{D}_{TV}(D_1, D_2)^2 - \mathrm{D}_{TV}(D_1, D^\star)^2}{2\mathrm{D}_{TV}(D_1, D_2)^2}, \quad \gamma_2^\star = 1 - \gamma_1^\star, \tag{11}$$

This solution is optimal provided that $\gamma_1^\star, \gamma_2^\star \geq 0$.

(b) ***Case** $n > 2$: For more than two pre-trained models, an explicit solution for the optimal combination coefficients $\boldsymbol{\gamma}^\star$ generally does not exist under the constraints $\gamma_i^\star \geq 0$. However, if we further impose $\gamma_i^\star > 0$ for all i, the optimal coefficients can be explicitly determined as:*

$$\boldsymbol{\gamma}^\star = \frac{\mathbf{H}^{-1}\mathbf{e}}{\mathbf{e}^\top \mathbf{H}^{-1}\mathbf{e}}, \tag{12}$$

where $\mathbf{H} \in \mathbb{R}^{n \times n}$ is a matrix with elements H_{ij} determined by:

$$H_{ij} = \mathrm{D}_{TV}(D_i, D^\star)^2 + \mathrm{D}_{TV}(D_j, D^\star)^2 - \mathrm{D}_{TV}(D_i, D_j)^2. \tag{13}$$

and $\mathbf{e}$ is an n-dimensional vector with all entries equal to 1.

Furthermore, Theorem 3 reveals an important insight: the smaller the total variation distance $\mathrm{D}_{\mathrm{TV}}(D_i, D^\star)$, the larger the corresponding weight $\gamma_i^\star$. In other words, pre-trained models closer to the target distribution receive higher weights in the optimal combination, ensuring that these models contribute more significantly to the proximal parameter and improve the approximation accuracy.

Retraining on new data. With the proximal parameter $\boldsymbol{\theta}^{\mathrm{P}}$ as the initial parameter of model $\boldsymbol{\phi}$, we proceed to retrain the model $\boldsymbol{\phi}$ on new data D. The training objective is to minimize the expected loss $\mathcal{J}(\boldsymbol{\theta})$ as in (2). Starting from $\boldsymbol{\theta}^{(0)} = \boldsymbol{\theta}^{\mathrm{P}}$, the model is expected to converge faster due to the informative initialization, as demonstrated in Theorem 2. Furthermore, its generalization error remains bounded as shown in Theorem 4.

4.3 Experimental Setting

In this section, we provide a comprehensive overview of our experimental setup, encompassing the models, datasets, baselines, metrics, and training details used to evaluate the effectiveness of our proposed SAIL method across different modalities, including natural language processing and computer vision tasks. Additional implementation details, including specific hyperparameters, and detailed model architectures, are provided in Appendix H.

Base Models. For the natural language processing sequence modeling task, we utilize the GPT-2 architecture (Radford et al., 2019), employing the nanoGPT[1] implementation. We consider models of

[1] https://github.com/karpathy/nanoGPT

varying sizes to assess the scalability of our method. Specifically, our base experiment configuration includes models with 6 layers and a hidden dimension of 384, amounting to approximately 21 million parameters. For the computer vision task, we employ convolutional neural network architectures, focusing on ResNet variants (He et al., 2016). We use the standard ResNet-18 models to evaluate the applicability of our method in the vision domain. Additionally, we consider modified version of ResNet-18 and ResNet-34. See more detailed configurations in Appendix H

Datasets. In the NLP domain, we use the OpenWebText (Gokaslan et al., 2019) and WikiText-103 (Merity et al., 2016) datasets for training and evaluation. These datasets are partitioned to simulate different training subsets, allowing us to train multiple models on different data partitions for the Proximal Parameter method. In the computer vision domain, we conduct experiments on standard image classification datasets: CIFAR-10, CIFAR-100 (Krizhevsky et al., 2009), and Tiny ImageNet (Le & Yang, 2015).

Methods. We pre-train ResNet models using both supervised and self-supervised learning paradigms, with the latter employing the BYOL framework (Grill et al., 2020).

Metrics. We measure performance using **top-1** and **top-5 accuracy** on the validation sets of CIFAR-10, CIFAR-100, and Tiny ImageNet. We also monitor training loss and convergence rates to assess the efficiency of different training methods.

4.4 Empirical Evaluation of SAIL's Efficacy

To evaluate the robustness and effectiveness of our SAIL method across different data distributions and scenarios, we conducted a series of experiments focusing on data distribution effects, overlap impacts, and cross-dataset generalization.

Dataset Partitioning and Distributional Analysis We partitioned our dataset into three distinct subsets (D_1, D_2, and D_t) based on feature segmentation using mean token values. This partitioning strategy, inspired by the theoretical foundations of our method, allows us to simulate diverse data distributions commonly encountered in real-world scenarios. We computed the mean token value for blocks of data and used the 33rd and 66th percentiles as thresholds, a choice motivated by our aim to create balanced yet distinct subsets. Samples with mean token values below the lower threshold were assigned to D_1, those between the thresholds to D_2, and those above the upper threshold to D_t, resulting in three datasets with distinct distributions that serve as an ideal testbed for our SAIL method.

As illustrated in Figure 2a, a t-SNE visualization shows that these datasets form three clearly separated clusters, empirically confirming the effectiveness of our theoretically-motivated feature-based splitting approach.

To demonstrate the superiority of SAIL over random initialization in practice, we trained two foundation models, $\boldsymbol{\theta}_1$ and $\boldsymbol{\theta}_2$, on D_1 and D_2, respectively. Our objective was to merge these models using our SAIL method and evaluate the convergence speed of the merged model on the new data partition D_t, thereby testing the practical implications of our theoretical framework. As shown in Figure 2b, the validation loss for random initialization is 10.8866, significantly higher than the minimum loss of 4.9782 achieved by our SAIL method. This substantial gap not only demonstrates the effectiveness of our approach in providing a more favorable initialization point in the loss landscape but also validates our theoretical predictions about the benefits of informed parameter initialization.

We systematically explored the parameter space by merging $\boldsymbol{\theta}_1$ and $\boldsymbol{\theta}_2$ using 30 values of γ in the range $[-1, 2]$ with increments of 0.1. This comprehensive sweep allows us to empirically validate the theoretical predictions of the optimal combination coefficient γ^* as detailed in Theorem 3. Each merged model was then retrained on D_t for a small number of iterations (50, 100, and 200), and we recorded the validation loss, providing insights into both short-term and longer-term effects of our initialization strategy.

Figure 2b presents the validation loss after 50, 100, and 200 iterations of retraining for different values of γ. The optimal γ corresponds to the minimum validation loss, indicating the best merging ratio

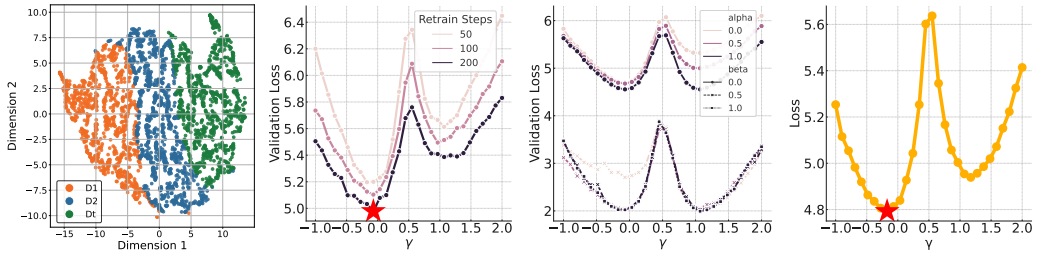

(a) t-SNE Visualization of D_1, D_2, and D_t (b) Validation Loss vs. γ (c) Validation Loss vs. γ (Overlaps) (d) Cross-Dataset Validation Loss

Figure 2: **Experimental Results:** (a) t-SNE visualization of datasets D_1, D_2, and D_t. (b) Validation loss after retraining as a function of merge ratio γ. (c) Validation loss on D_t vs. γ for various data overlaps. (d) Cross-dataset validation loss on WikiText-103.

for rapid convergence on D_t. This empirical finding aligns closely with our theoretical predictions, further validating the robustness of our approach.

Applying Theorem 3 to our experimental scenario, we compute the theoretical optimal γ^* using the Maximum Mean Discrepancy (MMD) distances between datasets: $\gamma^* = \frac{\text{MMD}(D_1,D_t)^2+\text{MMD}(D_1,D_2)^2-\text{MMD}(D_2,D_t)^2}{2\cdot\text{MMD}(D_1,D_2)^2} = -0.1244$. This theoretically derived γ^* value of -0.1244 closely aligns with the empirically observed optimal γ in Figure 2b, providing strong evidence for the practical applicability of our theoretical framework.

Impact of Data Overlap on SAIL To investigate the impact of data overlap, we defined parameters α and β. Here, α represents the overlap between D_1 and D_2, while β denotes the overlap of both D_1 and D_2 with D_t. These overlap fractions range from 0.0 to 1.0, encompassing scenarios from no overlap to full overlap.

For each combination of α and β, we trained separate models $\boldsymbol{\theta}_1$ and $\boldsymbol{\theta}_2$ on D_1 and D_2, respectively, and an optimal model $\boldsymbol{\theta}^\star$ on the target dataset D_t. We evaluated 30 equally spaced γ values in the range $[-1, 2]$ for merging $\boldsymbol{\theta}_1$ and $\boldsymbol{\theta}_2$. The merged models were then fine-tuned on D_t for 50 steps to assess the impact of additional training.

Our analysis revealed several key findings, as shown in Figure 2c:

(a) The optimal γ values concentrating near 0.0 and 1.0 suggest that the most effective interpolation often involves one model being slightly regularized by another. It is important to note that when γ is 0.5, the observed spike in performance does not necessarily indicate a rapid convergence to the global optimum.
(b) As the overlap between datasets increased, the validation loss curves exhibited greater symmetry around the optimal γ value. This symmetry suggests that both component models extracted similar features from the overlapping data.
(c) At lower overlap fractions, the asymmetry observed in the curves implies that one of the component models captured more generalizable features relevant to the target dataset D_t.

These observations are consistent with our theoretical considerations in Assumption 4, where the relationship between model parameters and data features influences the optimal merging strategy.

Cross-Dataset Transfer Analysis To assess SAIL's ability to leverage cross-dataset knowledge, we conducted experiments transferring models trained on OpenWebText to the WikiText-103 dataset. This setup tests the algorithm's capacity to generalize across datasets with different styles, vocabularies, and content structures.

We first trained two models, $\boldsymbol{\theta}_1$ and $\boldsymbol{\theta}_2$, on disjoint partitions D_1 and D_2 of OpenWebText. These partitions were created using a feature-based splitting approach that considers the mean token value of samples. We then used SAIL to initialize a model for fine-tuning on WikiText-103, which serves as our target dataset D_t.

Figure 2d presents the validation loss on WikiText-103 as a function of the merge ratio γ. The curve's shape and the existence of a clear optimal γ demonstrate SAIL's capacity to effectively

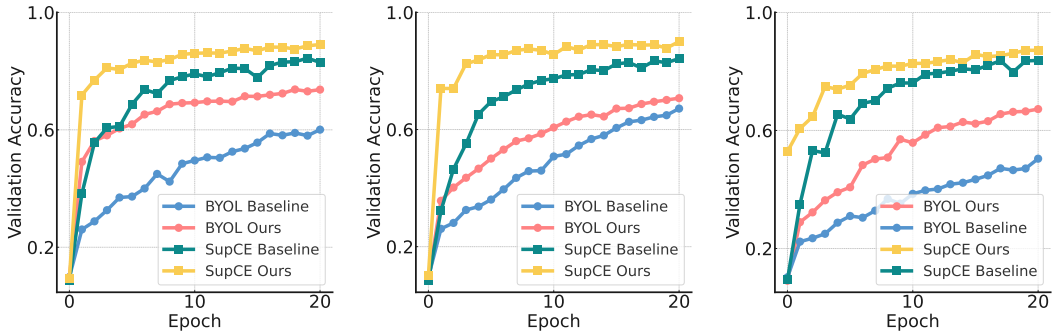

(a) ResNet-18 Modified (CIFAR-10) (b) Standard ResNet-18 (CIFAR-10) (c) ResNet-34 Modified (CIFAR-10)

Figure 3: **Accuracy in Different ResNet Configurations: (a)** Accuracy of ResNet-18 Modified trained with BYOL and SupCE on CIFAR-10. **(b)** Accuracy of standard ResNet-18 trained with BYOL and SupCE on CIFAR-10. **(c)** Accuracy of ResNet-34 Modified trained with BYOL and SupCE on CIFAR-10.

combine knowledge from disparate datasets, even when generalizing to a new domain with different stylistic and content characteristics.

4.5 Our Methods in Different Modality

To demonstrate the versatility and effectiveness of our proposed SAIL method beyond natural language processing, we extend our experiments to the computer vision domain. Specifically, we apply SAIL to convolutional neural network architectures, focusing on ResNet variants trained on image classification tasks. This section details the experimental setup, and results of applying SAIL to different ResNet models under both self-supervised and supervised learning paradigms.

We conduct experiments using three configurations of ResNet architectures: ResNet-18 (He et al., 2016), and ResNet-34. All models are trained on three datasets: CIFAR-10 (Krizhevsky et al., 2009), CIFAR-100 (Krizhevsky et al., 2009), and Tiny-ImageNet (Le & Yang, 2015).

Figure 3a illustrates the training performance of SAIL compared to baseline methods for ResNet-18 Modified across three datasets. Under both BYOL (self-supervised) and SupCE (supervised) paradigms, models initialized with SAIL demonstrate faster convergence and higher final accuracy compared to standard initialization and baseline transformation methods. This indicates that SAIL effectively leverages pre-trained parameters to provide a beneficial starting point for training, consistently across different datasets of varying complexity.

To assess the adaptability of our method to architectural variations, we applied SAIL to ResNet-18 Modified (Figure 3a), Standard ResNet-18 (Figure 3b) and ResNet-34 Modified (Figure 3c) on the CIFAR-10 dataset. In all cases, SAIL-initialized models outperform baselines in terms of convergence speed and final performance. The improvements are particularly pronounced under the SupCE paradigm, suggesting that supervised fine-tuning benefits significantly from our informed parameter initialization approach.

For additional results on CIFAR-100 and Tiny-ImageNet using ResNet-18 Modified, Standard ResNet-18 and ResNet-34 Modified, please refer to Appendix H.2.

5 Conclusion and Future Work

In this paper, we have introduced SAIL, a novel approach to accelerate the training of deep neural networks by leveraging the information from pre-trained counterparts. Our method comprises two primary components: (1) a parameter transformation technique that aligns the dimensions of pre-trained model parameters with the target architecture, and (2) a proximal parameter integration and retraining strategy that efficiently merges these transformed parameters to initialize new models. Our approach significantly reduces training time and computational resources while maintaining or enhancing model performance on downstream tasks.

REFERENCES

Winogrande: An adversarial winograd schema challenge at scale. 2019.

Yoshua Bengio, Jérôme Louradour, Ronan Collobert, and Jason Weston. Curriculum learning. In *Proceedings of the 26th annual international conference on machine learning*, pp. 41–48, 2009.

Yonatan Bisk, Rowan Zellers, Ronan Le Bras, Jianfeng Gao, and Yejin Choi. Piqa: Reasoning about physical commonsense in natural language. In *Thirty-Fourth AAAI Conference on Artificial Intelligence*, 2020.

Su Lin Blodgett, Solon Barocas, Hal Daumé III, and Hanna Wallach. Language (technology) is power: A critical survey of" bias" in nlp. *arXiv preprint arXiv:2005.14050*, 2020.

Tom Brown, Benjamin Mann, Nick Ryder, Melanie Subbiah, Jared D Kaplan, Prafulla Dhariwal, Arvind Neelakantan, Pranav Shyam, Girish Sastry, Amanda Askell, et al. Language models are few-shot learners. *Advances in neural information processing systems*, 33:1877–1901, 2020.

Tianqi Chen, Ian Goodfellow, and Jonathon Shlens. Net2net: Accelerating learning via knowledge transfer. *arXiv preprint arXiv:1511.05641*, 2015.

Tianqi Chen, Bing Xu, Chiyuan Zhang, and Carlos Guestrin. Training deep nets with sublinear memory cost. *arXiv preprint arXiv:1604.06174*, 2016.

Ting Chen, Simon Kornblith, Mohammad Norouzi, and Geoffrey Hinton. A simple framework for contrastive learning of visual representations. In *ICML*, 2020.

Rewon Child, Scott Gray, Alec Radford, and Ilya Sutskever. Generating long sequences with sparse transformers. *arXiv preprint arXiv:1904.10509*, 2019.

Aakanksha Chowdhery, Sharan Narang, Jacob Devlin, Maarten Bosma, Gaurav Mishra, Adam Roberts, Paul Barham, Hyung Won Chung, Charles Sutton, Sebastian Gehrmann, et al. Palm: Scaling language modeling with pathways. *Journal of Machine Learning Research*, 24(240):1–113, 2023.

Alexandra Chronopoulou, Jonas Pfeiffer, Joshua Maynez, Xinyi Wang, Sebastian Ruder, and Priyanka Agrawal. Language and task arithmetic with parameter-efficient layers for zero-shot summarization. *arXiv preprint arXiv:2311.09344*, 2023.

Peter Clark, Isaac Cowhey, Oren Etzioni, Tushar Khot, Ashish Sabharwal, Carissa Schoenick, and Oyvind Tafjord. Think you have solved question answering? try arc, the ai2 reasoning challenge. *arXiv:1803.05457v1*, 2018.

Tim Dettmers, Artidoro Pagnoni, Ari Holtzman, and Luke Zettlemoyer. Qlora: Efficient finetuning of quantized llms. *Advances in Neural Information Processing Systems*, 36, 2024.

Ahmad Faiz, Sotaro Kaneda, Ruhan Wang, Rita Osi, Parteek Sharma, Fan Chen, and Lei Jiang. Llmcarbon: Modeling the end-to-end carbon footprint of large language models. *arXiv preprint arXiv:2309.14393*, 2023.

Lijie Fan, Kaifeng Chen, Dilip Krishnan, Dina Katabi, Phillip Isola, and Yonglong Tian. Scaling laws of synthetic images for model training... for now. In *Proceedings of the IEEE/CVF Conference on Computer Vision and Pattern Recognition*, pp. 7382–7392, 2024.

Tommaso Furlanello, Zachary Lipton, Michael Tschannen, Laurent Itti, and Anima Anandkumar. Born again neural networks. In *International conference on machine learning*, pp. 1607–1616. PMLR, 2018.

Tianyu Gao, Adam Fisch, and Danqi Chen. Making pre-trained language models better few-shot learners. *arXiv preprint arXiv:2012.15723*, 2020.

Xavier Glorot and Yoshua Bengio. Understanding the difficulty of training deep feedforward neural networks. In *Proceedings of the thirteenth international conference on artificial intelligence and statistics*, pp. 249–256. JMLR Workshop and Conference Proceedings, 2010.

Aaron Gokaslan, Vanya Cohen, Ellie Pavlick, and Stefanie Tellex. Openwebtext corpus. http://Skylion007.github.io/OpenWebTextCorpus, 2019.

Linyuan Gong, Di He, Zhuohan Li, Tao Qin, Liwei Wang, and Tieyan Liu. Efficient training of bert by progressively stacking. In *International conference on machine learning*, pp. 2337–2346. PMLR, 2019.

Ariel Gordon, Elad Eban, Ofir Nachum, Bo Chen, Hao Wu, Tien-Ju Yang, and Edward Choi. Morphnet: Fast & simple resource-constrained structure learning of deep networks. In *Proceedings of the IEEE conference on computer vision and pattern recognition*, pp. 1586–1595, 2018.

Jianping Gou, Baosheng Yu, Stephen J Maybank, and Dacheng Tao. Knowledge distillation: A survey. *International Journal of Computer Vision*, 129(6):1789–1819, 2021.

Jean-Bastien Grill, Florian Strub, Florent Altché, Corentin Tallec, Pierre Richemond, Elena Buchatskaya, Carl Doersch, Bernardo Avila Pires, Zhaohan Guo, Mohammad Gheshlaghi Azar, et al. Bootstrap your own latent-a new approach to self-supervised learning. *Advances in neural information processing systems*, 33:21271–21284, 2020.

Dirk Groeneveld, Iz Beltagy, Pete Walsh, Akshita Bhagia, Rodney Kinney, Oyvind Tafjord, A. Jha, Hamish Ivison, Ian Magnusson, Yizhong Wang, Shane Arora, David Atkinson, Russell Authur, Khyathi Raghavi Chandu, Arman Cohan, Jennifer Dumas, Yanai Elazar, Yuling Gu, Jack Hessel, Tushar Khot, William Merrill, Jacob Daniel Morrison, Niklas Muennighoff, Aakanksha Naik, Crystal Nam, Matthew E. Peters, Valentina Pyatkin, Abhilasha Ravichander, Dustin Schwenk, Saurabh Shah, Will Smith, Emma Strubell, Nishant Subramani, Mitchell Wortsman, Pradeep Dasigi, Nathan Lambert, Kyle Richardson, Luke Zettlemoyer, Jesse Dodge, Kyle Lo, Luca Soldaini, Noah A. Smith, and Hanna Hajishirzi. Olmo: Accelerating the science of language models. *arXiv preprint*, 2024. URL https://api.semanticscholar.org/CorpusID:267365485.

Jia-Chen Gu, Hao-Xiang Xu, Jun-Yu Ma, Pan Lu, Zhen-Hua Ling, Kai-Wei Chang, and Nanyun Peng. Model editing can hurt general abilities of large language models. *arXiv preprint arXiv:2401.04700*, 2024.

Isabelle Guyon and André Elisseeff. An introduction to variable and feature selection. *Journal of machine learning research*, 3(Mar):1157–1182, 2003.

Kaiming He, Xiangyu Zhang, Shaoqing Ren, and Jian Sun. Delving deep into rectifiers: Surpassing human-level performance on imagenet classification. In *Proceedings of the IEEE international conference on computer vision*, pp. 1026–1034, 2015.

Kaiming He, Xiangyu Zhang, Shaoqing Ren, and Jian Sun. Deep residual learning for image recognition. In *Proceedings of the IEEE conference on computer vision and pattern recognition*, pp. 770–778, 2016.

Kaiming He, Haoqi Fan, Yuxin Wu, Saining Xie, and Ross Girshick. Momentum contrast for unsupervised visual representation learning. In *CVPR*, 2020.

Geoffrey Hinton, Oriol Vinyals, and Jeff Dean. Distilling the knowledge in a neural network. *arXiv preprint arXiv:1503.02531*, 2015.

Edward J Hu, Yelong Shen, Phillip Wallis, Zeyuan Allen-Zhu, Yuanzhi Li, Shean Wang, Lu Wang, and Weizhu Chen. Lora: Low-rank adaptation of large language models. *arXiv preprint arXiv:2106.09685*, 2021.

Zixian Huang, Wenhao Zhu, Gong Cheng, Lei Li, and Fei Yuan. Mindmerger: Efficient boosting llm reasoning in non-english languages. *arXiv preprint arXiv:2405.17386*, 2024.

Gabriel Ilharco, Marco Tulio Ribeiro, Mitchell Wortsman, Suchin Gururangan, Ludwig Schmidt, Hannaneh Hajishirzi, and Ali Farhadi. Editing models with task arithmetic. *arXiv preprint arXiv:2212.04089*, 2022.

Ziwei Ji, Nayeon Lee, Rita Frieske, Tiezheng Yu, Dan Su, Yan Xu, Etsuko Ishii, Ye Jin Bang, Andrea Madotto, and Pascale Fung. Survey of hallucination in natural language generation. *ACM Computing Surveys*, 55(12):1–38, 2023.

Angela H Jiang, Daniel L-K Wong, Giulio Zhou, David G Andersen, Jeffrey Dean, Gregory R Ganger, Gauri Joshi, Michael Kaminksy, Michael Kozuch, Zachary C Lipton, et al. Accelerating deep learning by focusing on the biggest losers. *arXiv preprint arXiv:1910.00762*, 2019.

Xiaoqi Jiao, Yichun Yin, Lifeng Shang, Xin Jiang, Xiao Chen, Linlin Li, Fang Wang, and Qun Liu. Tinybert: Distilling bert for natural language understanding. *arXiv preprint arXiv:1909.10351*, 2019.

Matt Gardner Johannes Welbl, Nelson F. Liu. Crowdsourcing multiple choice science questions. 2017.

Jean Kaddour, Joshua Harris, Maximilian Mozes, Herbie Bradley, Roberta Raileanu, and Robert McHardy. Challenges and applications of large language models. *arXiv preprint arXiv:2307.10169*, 2023.

Alex Krizhevsky, Geoffrey Hinton, et al. Learning multiple layers of features from tiny images. 2009.

Ya Le and Xuan Yang. Tiny imagenet visual recognition challenge. *CS 231N*, 7(7):3, 2015.

Changlin Li, Bohan Zhuang, Guangrun Wang, Xiaodan Liang, Xiaojun Chang, and Yi Yang. Automated progressive learning for efficient training of vision transformers. In *Proceedings of the IEEE/CVF Conference on Computer Vision and Pattern Recognition*, pp. 12486–12496, 2022.

Deyuan Liu, Zecheng Wang, Bingning Wang, Weipeng Chen, Chunshan Li, Zhiying Tu, Dianhui Chu, Bo Li, and Dianbo Sui. Checkpoint merging via bayesian optimization in llm pretraining. *arXiv preprint arXiv:2403.19390*, 2024.

Haochen Liu and X Zhao. Self-supervised learning for alleviating selection bias in recommendation systems. In *Proc. 2nd Int. Workshop Ind. Recommendation Syst.(Conjunction KDD 2021)*, 2021.

Hong Liu, Zhiyuan Li, David Hall, Percy Liang, and Tengyu Ma. Sophia: A scalable stochastic second-order optimizer for language model pre-training. *arXiv preprint arXiv:2305.14342*, 2023.

Yinhan Liu. Roberta: A robustly optimized bert pretraining approach. *arXiv preprint arXiv:1907.11692*, 2019.

Nanye Ma, Mark Goldstein, Michael S Albergo, Nicholas M Boffi, Eric Vanden-Eijnden, and Saining Xie. SiT: Exploring flow and diffusion-based generative models with scalable interpolant transformers. 2024.

Kevin Meng, David Bau, Alex Andonian, and Yonatan Belinkov. Locating and editing factual associations in gpt. *Advances in Neural Information Processing Systems*, 35:17359–17372, 2022.

Stephen Merity, Caiming Xiong, James Bradbury, and Richard Socher. Pointer sentinel mixture models, 2016.

Paulius Micikevicius, Sharan Narang, Jonah Alben, Gregory Diamos, Erich Elsen, David Garcia, Boris Ginsburg, Michael Houston, Oleksii Kuchaiev, Ganesh Venkatesh, et al. Mixed precision training. *arXiv preprint arXiv:1710.03740*, 2017.

Sören Mindermann, Jan M Brauner, Muhammed T Razzak, Mrinank Sharma, Andreas Kirsch, Winnie Xu, Benedikt Höltgen, Aidan N Gomez, Adrien Morisot, Sebastian Farquhar, et al. Prioritized training on points that are learnable, worth learning, and not yet learnt. In *International Conference on Machine Learning*, pp. 15630–15649. PMLR, 2022.

OpenAI, :, Josh Achiam, Steven Adler, Sandhini Agarwal, Lama Ahmad, Ilge Akkaya, Florencia Leoni Aleman, Diogo Almeida, Janko Altenschmidt, Sam Altman, Shyamal Anadkat, Red Avila, Igor Babuschkin, Suchir Balaji, Valerie Balcom, Paul Baltescu, Haiming Bao, Mo Bavarian, Jeff Belgum, Irwan Bello, Jake Berdine, Gabriel Bernadett-Shapiro, Christopher Berner, Lenny Bogdonoff, Oleg Boiko, Madelaine Boyd, Anna-Luisa Brakman, Greg Brockman, Tim Brooks, Miles Brundage, Kevin Button, Trevor Cai, Rosie Campbell, Andrew Cann, Brittany Carey, Chelsea Carlson, Rory Carmichael, Brooke Chan, Che Chang, Fotis Chantzis, Derek Chen, Sully Chen, Ruby Chen, Jason Chen, Mark Chen, Ben Chess, Chester Cho, Casey Chu, Hyung Won Chung, Dave Cummings, Jeremiah Currier, Yunxing Dai, Cory Decareaux, Thomas Degry, Noah

Deutsch, Damien Deville, Arka Dhar, David Dohan, Steve Dowling, Sheila Dunning, Adrien Ecoffet, Atty Eleti, Tyna Eloundou, David Farhi, Liam Fedus, Niko Felix, Simón Posada Fishman, Juston Forte, Isabella Fulford, Leo Gao, Elie Georges, Christian Gibson, Vik Goel, Tarun Gogineni, Gabriel Goh, Rapha Gontijo-Lopes, Jonathan Gordon, Morgan Grafstein, Scott Gray, Ryan Greene, Joshua Gross, Shixiang Shane Gu, Yufei Guo, Chris Hallacy, Jesse Han, Jeff Harris, Yuchen He, Mike Heaton, Johannes Heidecke, Chris Hesse, Alan Hickey, Wade Hickey, Peter Hoeschele, Brandon Houghton, Kenny Hsu, Shengli Hu, Xin Hu, Joost Huizinga, Shantanu Jain, Shawn Jain, Joanne Jang, Angela Jiang, Roger Jiang, Haozhun Jin, Denny Jin, Shino Jomoto, Billie Jonn, Heewoo Jun, Tomer Kaftan, Łukasz Kaiser, Ali Kamali, Ingmar Kanitscheider, Nitish Shirish Keskar, Tabarak Khan, Logan Kilpatrick, Jong Wook Kim, Christina Kim, Yongjik Kim, Hendrik Kirchner, Jamie Kiros, Matt Knight, Daniel Kokotajlo, Łukasz Kondraciuk, Andrew Kondrich, Aris Konstantinidis, Kyle Kosic, Gretchen Krueger, Vishal Kuo, Michael Lampe, Ikai Lan, Teddy Lee, Jan Leike, Jade Leung, Daniel Levy, Chak Ming Li, Rachel Lim, Molly Lin, Stephanie Lin, Mateusz Litwin, Theresa Lopez, Ryan Lowe, Patricia Lue, Anna Makanju, Kim Malfacini, Sam Manning, Todor Markov, Yaniv Markovski, Bianca Martin, Katie Mayer, Andrew Mayne, Bob McGrew, Scott Mayer McKinney, Christine McLeavey, Paul McMillan, Jake McNeil, David Medina, Aalok Mehta, Jacob Menick, Luke Metz, Andrey Mishchenko, Pamela Mishkin, Vinnie Monaco, Evan Morikawa, Daniel Mossing, Tong Mu, Mira Murati, Oleg Murk, David Mély, Ashvin Nair, Reiichiro Nakano, Rajeev Nayak, Arvind Neelakantan, Richard Ngo, Hyeonwoo Noh, Long Ouyang, Cullen O'Keefe, Jakub Pachocki, Alex Paino, Joe Palermo, Ashley Pantuliano, Giambattista Parascandolo, Joel Parish, Emy Parparita, Alex Passos, Mikhail Pavlov, Andrew Peng, Adam Perelman, Filipe de Avila Belbute Peres, Michael Petrov, Henrique Ponde de Oliveira Pinto, Michael, Pokorny, Michelle Pokrass, Vitchyr Pong, Tolly Powell, Alethea Power, Boris Power, Elizabeth Proehl, Raul Puri, Alec Radford, Jack Rae, Aditya Ramesh, Cameron Raymond, Francis Real, Kendra Rimbach, Carl Ross, Bob Rotsted, Henri Roussez, Nick Ryder, Mario Saltarelli, Ted Sanders, Shibani Santurkar, Girish Sastry, Heather Schmidt, David Schnurr, John Schulman, Daniel Selsam, Kyla Sheppard, Toki Sherbakov, Jessica Shieh, Sarah Shoker, Pranav Shyam, Szymon Sidor, Eric Sigler, Maddie Simens, Jordan Sitkin, Katarina Slama, Ian Sohl, Benjamin Sokolowsky, Yang Song, Natalie Staudacher, Felipe Petroski Such, Natalie Summers, Ilya Sutskever, Jie Tang, Nikolas Tezak, Madeleine Thompson, Phil Tillet, Amin Tootoonchian, Elizabeth Tseng, Preston Tuggle, Nick Turley, Jerry Tworek, Juan Felipe Cerón Uribe, Andrea Vallone, Arun Vijayvergiya, Chelsea Voss, Carroll Wainwright, Justin Jay Wang, Alvin Wang, Ben Wang, Jonathan Ward, Jason Wei, CJ Weinmann, Akila Welihinda, Peter Welinder, Jiayi Weng, Lilian Weng, Matt Wiethoff, Dave Willner, Clemens Winter, Samuel Wolrich, Hannah Wong, Lauren Workman, Sherwin Wu, Jeff Wu, Michael Wu, Kai Xiao, Tao Xu, Sarah Yoo, Kevin Yu, Qiming Yuan, Wojciech Zaremba, Rowan Zellers, Chong Zhang, Marvin Zhang, Shengjia Zhao, Tianhao Zheng, Juntang Zhuang, William Zhuk, and Barret Zoph. Gpt-4 technical report, 2023.

Guillermo Ortiz-Jimenez, Alessandro Favero, and Pascal Frossard. Task arithmetic in the tangent space: Improved editing of pre-trained models. *Advances in Neural Information Processing Systems*, 36, 2024.

Yu Pan, Ye Yuan, Yichun Yin, Jiaxin Shi, Zenglin Xu, Ming Zhang, Lifeng Shang, Xin Jiang, and Qun Liu. Preparing lessons for progressive training on language models. In *Proceedings of the AAAI Conference on Artificial Intelligence*, volume 38, pp. 18860–18868, 2024.

Yujia Qin, Yankai Lin, Jing Yi, Jiajie Zhang, Xu Han, Zhengyan Zhang, Yusheng Su, Zhiyuan Liu, Peng Li, Maosong Sun, et al. Knowledge inheritance for pre-trained language models. *arXiv preprint arXiv:2105.13880*, 2021.

Alec Radford, Jeffrey Wu, Rewon Child, David Luan, Dario Amodei, Ilya Sutskever, et al. Language models are unsupervised multitask learners. *OpenAI blog*, 1(8):9, 2019.

Melissa Roemmele, Cosmin Adrian Bejan, and Andrew S Gordon. Choice of plausible alternatives: An evaluation of commonsense causal reasoning. In *2011 AAAI Spring Symposium Series*, 2011. URL https://people.ict.usc.edu/~gordon/publications/AAAI-SPRING11A.PDF.

Mohammad Samragh, Iman Mirzadeh, Keivan Alizadeh Vahid, Fartash Faghri, Minsik Cho, Moin Nabi, Devang Naik, and Mehrdad Farajtabar. Scaling smart: Accelerating large language model pre-training with small model initialization. *arXiv preprint arXiv:2409.12903*, 2024.

Victor Sanh, Lysandre Debut, Julien Chaumond, and Thomas Wolf. Distilbert, a distilled version of bert: smaller, faster, cheaper and lighter. *arXiv preprint arXiv:1910.01108*, 2019.

Noam Shazeer and Mitchell Stern. Adafactor: Adaptive learning rates with sublinear memory cost. In *International Conference on Machine Learning*, pp. 4596–4604. PMLR, 2018.

Haobo SONG, Hao Zhao, Soumajit Majumder, and Tao Lin. Increasing model capacity for free: A simple strategy for parameter efficient fine-tuning. In *The Twelfth International Conference on Learning Representations*, 2024. URL https://openreview.net/forum?id=H3IUunLy8s.

Jie Song, Ying Chen, Jingwen Ye, and Mingli Song. Spot-adaptive knowledge distillation. *IEEE Transactions on Image Processing*, 31:3359–3370, 2022.

Emma Strubell, Ananya Ganesh, and Andrew McCallum. Energy and policy considerations for modern deep learning research. In *Proceedings of the AAAI conference on artificial intelligence*, volume 34, pp. 13693–13696, 2020.

Chen Sun, Abhinav Shrivastava, Saurabh Singh, and Abhinav Gupta. Revisiting unreasonable effectiveness of data in deep learning era. In *Proceedings of the IEEE international conference on computer vision*, pp. 843–852, 2017.

Gemini Team, Rohan Anil, Sebastian Borgeaud, Yonghui Wu, Jean-Baptiste Alayrac, Jiahui Yu, Radu Soricut, Johan Schalkwyk, Andrew M. Dai, Anja Hauth, Katie Millican, David Silver, Slav Petrov, Melvin Johnson, Ioannis Antonoglou, Julian Schrittwieser, Amelia Glaese, Jilin Chen, Emily Pitler, Timothy Lillicrap, Angeliki Lazaridou, Orhan Firat, James Molloy, Michael Isard, Paul R. Barham, Tom Hennigan, Benjamin Lee, Fabio Viola, Malcolm Reynolds, Yuanzhong Xu, Ryan Doherty, Eli Collins, Clemens Meyer, Eliza Rutherford, Erica Moreira, Kareem Ayoub, Megha Goel, George Tucker, Enrique Piqueras, Maxim Krikun, Iain Barr, Nikolay Savinov, Ivo Danihelka, Becca Roelofs, Anaïs White, Anders Andreassen, Tamara von Glehn, Lakshman Yagati, Mehran Kazemi, Lucas Gonzalez, Misha Khalman, Jakub Sygnowski, Alexandre Frechette, Charlotte Smith, Laura Culp, Lev Proleev, Yi Luan, Xi Chen, James Lottes, Nathan Schucher, Federico Lebron, Alban Rrustemi, Natalie Clay, Phil Crone, Tomas Kocisky, Jeffrey Zhao, Bartek Perz, Dian Yu, Heidi Howard, Adam Bloniarz, Jack W. Rae, Han Lu, Laurent Sifre, Marcello Maggioni, Fred Alcober, Dan Garrette, Megan Barnes, Shantanu Thakoor, Jacob Austin, Gabriel Barth-Maron, William Wong, Rishabh Joshi, Rahma Chaabouni, Deeni Fatiha, Arun Ahuja, Ruibo Liu, Yunxuan Li, Sarah Cogan, Jeremy Chen, Chao Jia, Chenjie Gu, Qiao Zhang, Jordan Grimstad, Ale Jakse Hartman, Martin Chadwick, Gaurav Singh Tomar, Xavier Garcia, Evan Senter, Emanuel Taropa, Thanumalayan Sankaranarayana Pillai, Jacob Devlin, Michael Laskin, Diego de Las Casas, Dasha Valter, Connie Tao, Lorenzo Blanco, Adrià Puigdomènech Badia, David Reitter, Mianna Chen, Jenny Brennan, Clara Rivera, Sergey Brin, Shariq Iqbal, Gabriela Surita, Jane Labanowski, Abhi Rao, Stephanie Winkler, Emilio Parisotto, Yiming Gu, Kate Olszewska, Yujing Zhang, Ravi Addanki, Antoine Miech, Annie Louis, Laurent El Shafey, Denis Teplyashin, Geoff Brown, Elliot Catt, Nithya Attaluri, Jan Balaguer, Jackie Xiang, Pidong Wang, Zoe Ashwood, Anton Briukhov, Albert Webson, Sanjay Ganapathy, Smit Sanghavi, Ajay Kannan, Ming-Wei Chang, Axel Stjerngren, Josip Djolonga, Yuting Sun, Ankur Bapna, Matthew Aitchison, Pedram Pejman, Henryk Michalewski, Tianhe Yu, Cindy Wang, Juliette Love, Junwhan Ahn, Dawn Bloxwich, Kehang Han, Peter Humphreys, Thibault Sellam, James Bradbury, Varun Godbole, Sina Samangooei, Bogdan Damoc, Alex Kaskasoli, Sébastien M. R. Arnold, Vijay Vasudevan, Shubham Agrawal, Jason Riesa, Dmitry Lepikhin, Richard Tanburn, Srivatsan Srinivasan, Hyeontaek Lim, Sarah Hodkinson, Pranav Shyam, Johan Ferret, Steven Hand, Ankush Garg, Tom Le Paine, Jian Li, Yujia Li, Minh Giang, Alexander Neitz, Zaheer Abbas, Sarah York, Machel Reid, Elizabeth Cole, Aakanksha Chowdhery, Dipanjan Das, Dominika Rogozińska, Vitaly Nikolaev, Pablo Sprechmann, Zachary Nado, Lukas Zilka, Flavien Prost, Luheng He, Marianne Monteiro, Gaurav Mishra, Chris Welty, Josh Newlan, Dawei Jia, Miltiadis Allamanis, Clara Huiyi Hu, Raoul de Liedekerke, Justin Gilmer, Carl Saroufim, Shruti Rijhwani, Shaobo Hou, Disha Shrivastava, Anirudh Baddepudi, Alex Goldin, Adnan Ozturel, Albin Cassirer, Yunhan Xu, Daniel Sohn, Devendra Sachan, Reinald Kim Amplayo, Craig Swanson, Dessie Petrova, Shashi Narayan, Arthur Guez, Siddhartha Brahma, Jessica Landon, Miteyan Patel, Ruizhe Zhao, Kevin Villela, Luyu Wang, Wenhao Jia, Matthew Rahtz, Mai Giménez, Legg Yeung, Hanzhao Lin, James Keeling, Petko Georgiev, Diana Mincu, Boxi Wu, Salem Haykal, Rachel Saputro, Kiran Vodrahalli, James Qin, Zeynep Cankara, Abhanshu Sharma, Nick Fernando, Will Hawkins, Behnam Neyshabur,

Solomon Kim, Adrian Hutter, Priyanka Agrawal, Alex Castro-Ros, George van den Driessche, Tao Wang, Fan Yang, Shuo yiin Chang, Paul Komarek, Ross McIlroy, Mario Lučić, Guodong Zhang, Wael Farhan, Michael Sharman, Paul Natsev, Paul Michel, Yong Cheng, Yamini Bansal, Siyuan Qiao, Kris Cao, Siamak Shakeri, Christina Butterfield, Justin Chung, Paul Kishan Rubenstein, Shivani Agrawal, Arthur Mensch, Kedar Soparkar, Karel Lenc, Timothy Chung, Aedan Pope, Loren Maggiore, Jackie Kay, Priya Jhakra, Shibo Wang, Joshua Maynez, Mary Phuong, Taylor Tobin, Andrea Tacchetti, Maja Trebacz, Kevin Robinson, Yash Katariya, Sebastian Riedel, Paige Bailey, Kefan Xiao, Nimesh Ghelani, Lora Aroyo, Ambrose Slone, Neil Houlsby, Xuehan Xiong, Zhen Yang, Elena Gribovskaya, Jonas Adler, Mateo Wirth, Lisa Lee, Music Li, Thais Kagohara, Jay Pavagadhi, Sophie Bridgers, Anna Bortsova, Sanjay Ghemawat, Zafarali Ahmed, Tianqi Liu, Richard Powell, Vijay Bolina, Mariko Iinuma, Polina Zablotskaia, James Besley, Da-Woon Chung, Timothy Dozat, Ramona Comanescu, Xiance Si, Jeremy Greer, Guolong Su, Martin Polacek, Raphaël Lopez Kaufman, Simon Tokumine, Hexiang Hu, Elena Buchatskaya, Yingjie Miao, Mohamed Elhawaty, Aditya Siddhant, Nenad Tomasev, Jinwei Xing, Christina Greer, Helen Miller, Shereen Ashraf, Aurko Roy, Zizhao Zhang, Ada Ma, Angelos Filos, Milos Besta, Rory Blevins, Ted Klimenko, Chih-Kuan Yeh, Soravit Changpinyo, Jiaqi Mu, Oscar Chang, Mantas Pajarskas, Carrie Muir, Vered Cohen, Charline Le Lan, Krishna Haridasan, Amit Marathe, Steven Hansen, Sholto Douglas, Rajkumar Samuel, Mingqiu Wang, Sophia Austin, Chang Lan, Jiepu Jiang, Justin Chiu, Jaime Alonso Lorenzo, Lars Lowe Sjösund, Sébastien Cevey, Zach Gleicher, Thi Avrahami, Anudhyan Boral, Hansa Srinivasan, Vittorio Selo, Rhys May, Konstantinos Aisopos, Léonard Hussenot, Livio Baldini Soares, Kate Baumli, Michael B. Chang, Adrià Recasens, Ben Caine, Alexander Pritzel, Filip Pavetic, Fabio Pardo, Anita Gergely, Justin Frye, Vinay Ramasesh, Dan Horgan, Kartikeya Badola, Nora Kassner, Subhrajit Roy, Ethan Dyer, Víctor Campos, Alex Tomala, Yunhao Tang, Dalia El Badawy, Elspeth White, Basil Mustafa, Oran Lang, Abhishek Jindal, Sharad Vikram, Zhitao Gong, Sergi Caelles, Ross Hemsley, Gregory Thornton, Fangxiaoyu Feng, Wojciech Stokowiec, Ce Zheng, Phoebe Thacker, Çağlar Ünlü, Zhishuai Zhang, Mohammad Saleh, James Svensson, Max Bileschi, Piyush Patil, Ankesh Anand, Roman Ring, Katerina Tsihlas, Arpi Vezer, Marco Selvi, Toby Shevlane, Mikel Rodriguez, Tom Kwiatkowski, Samira Daruki, Keran Rong, Allan Dafoe, Nicholas FitzGerald, Keren Gu-Lemberg, Mina Khan, Lisa Anne Hendricks, Marie Pellat, Vladimir Feinberg, James Cobon-Kerr, Tara Sainath, Maribeth Rauh, Sayed Hadi Hashemi, Richard Ives, Yana Hasson, YaGuang Li, Eric Noland, Yuan Cao, Nathan Byrd, Le Hou, Qingze Wang, Thibault Sottiaux, Michela Paganini, Jean-Baptiste Lespiau, Alexandre Moufarek, Samer Hassan, Kaushik Shivakumar, Joost van Amersfoort, Amol Mandhane, Pratik Joshi, Anirudh Goyal, Matthew Tung, Andrew Brock, Hannah Sheahan, Vedant Misra, Cheng Li, Nemanja Rakićević, Mostafa Dehghani, Fangyu Liu, Sid Mittal, Junhyuk Oh, Seb Noury, Eren Sezener, Fantine Huot, Matthew Lamm, Nicola De Cao, Charlie Chen, Gamaleldin Elsayed, Ed Chi, Mahdis Mahdieh, Ian Tenney, Nan Hua, Ivan Petrychenko, Patrick Kane, Dylan Scandinaro, Rishub Jain, Jonathan Uesato, Romina Datta, Adam Sadovsky, Oskar Bunyan, Dominik Rabiej, Shimu Wu, John Zhang, Gautam Vasudevan, Edouard Leurent, Mahmoud Alnahlawi, Ionut Georgescu, Nan Wei, Ivy Zheng, Betty Chan, Pam G Rabinovitch, Piotr Stanczyk, Ye Zhang, David Steiner, Subhajit Naskar, Michael Azzam, Matthew Johnson, Adam Paszke, Chung-Cheng Chiu, Jaume Sanchez Elias, Afroz Mohiuddin, Faizan Muhammad, Jin Miao, Andrew Lee, Nino Vieillard, Sahitya Potluri, Jane Park, Elnaz Davoodi, Jiageng Zhang, Jeff Stanway, Drew Garmon, Abhijit Karmarkar, Zhe Dong, Jong Lee, Aviral Kumar, Luowei Zhou, Jonathan Evens, William Isaac, Zhe Chen, Johnson Jia, Anselm Levskaya, Zhenkai Zhu, Chris Gorgolewski, Peter Grabowski, Yu Mao, Alberto Magni, Kaisheng Yao, Javier Snaider, Norman Casagrande, Paul Suganthan, Evan Palmer, Geoffrey Irving, Edward Loper, Manaal Faruqui, Isha Arkatkar, Nanxin Chen, Izhak Shafran, Michael Fink, Alfonso Castaño, Irene Giannoumis, Wooyeol Kim, Mikołaj Rybiński, Ashwin Sreevatsa, Jennifer Prendki, David Soergel, Adrian Goedeckemeyer, Willi Gierke, Mohsen Jafari, Meenu Gaba, Jeremy Wiesner, Diana Gage Wright, Yawen Wei, Harsha Vashisht, Yana Kulizhskaya, Jay Hoover, Maigo Le, Lu Li, Chimezie Iwuanyanwu, Lu Liu, Kevin Ramirez, Andrey Khorlin, Albert Cui, Tian LIN, Marin Georgiev, Marcus Wu, Ricardo Aguilar, Keith Pallo, Abhishek Chakladar, Alena Repina, Xihui Wu, Tom van der Weide, Priya Ponnapalli, Caroline Kaplan, Jiri Simsa, Shuangfeng Li, Olivier Dousse, Fan Yang, Jeff Piper, Nathan Ie, Minnie Lui, Rama Pasumarthi, Nathan Lintz, Anitha Vijayakumar, Lam Nguyen Thiet, Daniel Andor, Pedro Valenzuela, Cosmin Paduraru, Daiyi Peng, Katherine Lee, Shuyuan Zhang, Somer Greene, Duc Dung Nguyen, Paula Kurylowicz, Sarmishta Velury, Sebastian Krause, Cassidy Hardin, Lucas Dixon, Lili Janzer, Kiam Choo, Ziqiang Feng, Biao Zhang, Achintya Singhal, Tejasi Latkar, Mingyang Zhang, Quoc Le, Elena Allica Abellan, Dayou Du, Dan McKinnon, Natasha Antropova, Tolga Bolukbasi, Orgad

Keller, David Reid, Daniel Finchelstein, Maria Abi Raad, Remi Crocker, Peter Hawkins, Robert Dadashi, Colin Gaffney, Sid Lall, Ken Franko, Egor Filonov, Anna Bulanova, Rémi Leblond, Vikas Yadav, Shirley Chung, Harry Askham, Luis C. Cobo, Kelvin Xu, Felix Fischer, Jun Xu, Christina Sorokin, Chris Alberti, Chu-Cheng Lin, Colin Evans, Hao Zhou, Alek Dimitriev, Hannah Forbes, Dylan Banarse, Zora Tung, Jeremiah Liu, Mark Omernick, Colton Bishop, Chintu Kumar, Rachel Sterneck, Ryan Foley, Rohan Jain, Swaroop Mishra, Jiawei Xia, Taylor Bos, Geoffrey Cideron, Ehsan Amid, Francesco Piccinno, Xingyu Wang, Praseem Banzal, Petru Gurita, Hila Noga, Premal Shah, Daniel J. Mankowitz, Alex Polozov, Nate Kushman, Victoria Krakovna, Sasha Brown, MohammadHossein Bateni, Dennis Duan, Vlad Firoiu, Meghana Thotakuri, Tom Natan, Anhad Mohananey, Matthieu Geist, Sidharth Mudgal, Sertan Girgin, Hui Li, Jiayu Ye, Ofir Roval, Reiko Tojo, Michael Kwong, James Lee-Thorp, Christopher Yew, Quan Yuan, Sumit Bagri, Danila Sinopalnikov, Sabela Ramos, John Mellor, Abhishek Sharma, Aliaksei Severyn, Jonathan Lai, Kathy Wu, Heng-Tze Cheng, David Miller, Nicolas Sonnerat, Denis Vnukov, Rory Greig, Jennifer Beattie, Emily Caveness, Libin Bai, Julian Eisenschlos, Alex Korchemniy, Tomy Tsai, Mimi Jasarevic, Weize Kong, Phuong Dao, Zeyu Zheng, Frederick Liu, Fan Yang, Rui Zhu, Mark Geller, Tian Huey Teh, Jason Sanmiya, Evgeny Gladchenko, Nejc Trdin, Andrei Sozanschi, Daniel Toyama, Evan Rosen, Sasan Tavakkol, Linting Xue, Chen Elkind, Oliver Woodman, John Carpenter, George Papamakarios, Rupert Kemp, Sushant Kafle, Tanya Grunina, Rishika Sinha, Alice Talbert, Abhimanyu Goyal, Diane Wu, Denese Owusu-Afriyie, Cosmo Du, Chloe Thornton, Jordi Pont-Tuset, Pradyumna Narayana, Jing Li, Sabaer Fatehi, John Wieting, Omar Ajmeri, Benigno Uria, Tao Zhu, Yeongil Ko, Laura Knight, Amélie Héliou, Ning Niu, Shane Gu, Chenxi Pang, Dustin Tran, Yeqing Li, Nir Levine, Ariel Stolovich, Norbert Kalb, Rebeca Santamaria-Fernandez, Sonam Goenka, Wenny Yustalim, Robin Strudel, Ali Elqursh, Balaji Lakshminarayanan, Charlie Deck, Shyam Upadhyay, Hyo Lee, Mike Dusenberry, Zonglin Li, Xuezhi Wang, Kyle Levin, Raphael Hoffmann, Dan Holtmann-Rice, Olivier Bachem, Summer Yue, Sho Arora, Eric Malmi, Daniil Mirylenka, Qijun Tan, Christy Koh, Soheil Hassas Yeganeh, Siim Põder, Steven Zheng, Francesco Pongetti, Mukarram Tariq, Yanhua Sun, Lucian Ionita, Mojtaba Seyedhosseini, Pouya Tafti, Ragha Kotikalapudi, Zhiyu Liu, Anmol Gulati, Jasmine Liu, Xinyu Ye, Bart Chrzaszcz, Lily Wang, Nikhil Sethi, Tianrun Li, Ben Brown, Shreya Singh, Wei Fan, Aaron Parisi, Joe Stanton, Chenkai Kuang, Vinod Koverkathu, Christopher A. Choquette-Choo, Yunjie Li, TJ Lu, Abe Ittycheriah, Prakash Shroff, Pei Sun, Mani Varadarajan, Sanaz Bahargam, Rob Willoughby, David Gaddy, Ishita Dasgupta, Guillaume Desjardins, Marco Cornero, Brona Robenek, Bhavishya Mittal, Ben Albrecht, Ashish Shenoy, Fedor Moiseev, Henrik Jacobsson, Alireza Ghaffarkhah, Morgane Rivière, Alanna Walton, Clément Crepy, Alicia Parrish, Yuan Liu, Zongwei Zhou, Clement Farabet, Carey Radebaugh, Praveen Srinivasan, Claudia van der Salm, Andreas Fidjeland, Salvatore Scellato, Eri Latorre-Chimoto, Hanna Klimczak-Plucińska, David Bridson, Dario de Cesare, Tom Hudson, Piermaria Mendolicchio, Lexi Walker, Alex Morris, Ivo Penchev, Matthew Mauger, Alexey Guseynov, Alison Reid, Seth Odoom, Lucia Loher, Victor Cotruta, Madhavi Yenugula, Dominik Grewe, Anastasia Petrushkina, Tom Duerig, Antonio Sanchez, Steve Yadlowsky, Amy Shen, Amir Globerson, Adam Kurzrok, Lynette Webb, Sahil Dua, Dong Li, Preethi Lahoti, Surya Bhupatiraju, Dan Hurt, Haroon Qureshi, Ananth Agarwal, Tomer Shani, Matan Eyal, Anuj Khare, Shreyas Rammohan Belle, Lei Wang, Chetan Tekur, Mihir Sanjay Kale, Jinliang Wei, Ruoxin Sang, Brennan Saeta, Tyler Liechty, Yi Sun, Yao Zhao, Stephan Lee, Pandu Nayak, Doug Fritz, Manish Reddy Vuyyuru, John Aslanides, Nidhi Vyas, Martin Wicke, Xiao Ma, Taylan Bilal, Evgenii Eltyshev, Daniel Balle, Nina Martin, Hardie Cate, James Manyika, Keyvan Amiri, Yelin Kim, Xi Xiong, Kai Kang, Florian Luisier, Nilesh Tripuraneni, David Madras, Mandy Guo, Austin Waters, Oliver Wang, Joshua Ainslie, Jason Baldridge, Han Zhang, Garima Pruthi, Jakob Bauer, Feng Yang, Riham Mansour, Jason Gelman, Yang Xu, George Polovets, Ji Liu, Honglong Cai, Warren Chen, XiangHai Sheng, Emily Xue, Sherjil Ozair, Adams Yu, Christof Angermueller, Xiaowei Li, Weiren Wang, Julia Wiesinger, Emmanouil Koukoumidis, Yuan Tian, Anand Iyer, Madhu Gurumurthy, Mark Goldenson, Parashar Shah, MK Blake, Hongkun Yu, Anthony Urbanowicz, Jennimaria Palomaki, Chrisantha Fernando, Kevin Brooks, Ken Durden, Harsh Mehta, Nikola Momchev, Elahe Rahimtoroghi, Maria Georgaki, Amit Raul, Sebastian Ruder, Morgan Redshaw, Jinhyuk Lee, Komal Jalan, Dinghua Li, Ginger Perng, Blake Hechtman, Parker Schuh, Milad Nasr, Mia Chen, Kieran Milan, Vladimir Mikulik, Trevor Strohman, Juliana Franco, Tim Green, Demis Hassabis, Koray Kavukcuoglu, Jeffrey Dean, and Oriol Vinyals. Gemini: A family of highly capable multimodal models, 2023.

Pala Tej Deep, Rishabh Bhardwaj, and Soujanya Poria. DELLA-Merging: Reducing Interference in Model Merging through Magnitude-Based Sampling. *arXiv e-prints*, art. arXiv:2406.11617, June 2024.

Yonglong Tian, Dilip Krishnan, and Phillip Isola. Contrastive multiview coding. In *Computer Vision–ECCV 2020: 16th European Conference, Glasgow, UK, August 23–28, 2020, Proceedings, Part XI 16*, pp. 776–794. Springer, 2020.

Hugo Touvron, Louis Martin, Kevin Stone, Peter Albert, Amjad Almahairi, Yasmine Babaei, Nikolay Bashlykov, Soumya Batra, Prajjwal Bhargava, Shruti Bhosale, et al. Llama 2: Open foundation and fine-tuned chat models. *arXiv preprint arXiv:2307.09288*, 2023.

Guangrun Wang, Keze Wang, Guangcong Wang, Philip HS Torr, and Liang Lin. Solving inefficiency of self-supervised representation learning. In *Proceedings of the IEEE/CVF International Conference on Computer Vision*, pp. 9505–9515, 2021.

Peihao Wang, Rameswar Panda, Lucas Torroba Hennigen, Philip Greengard, Leonid Karlinsky, Rogerio Feris, David Daniel Cox, Zhangyang Wang, and Yoon Kim. Learning to grow pretrained models for efficient transformer training. *arXiv preprint arXiv:2303.00980*, 2023a.

Peihao Wang, Rameswar Panda, and Zhangyang Wang. Data efficient neural scaling law via model reusing. In *International Conference on Machine Learning*, pp. 36193–36204. PMLR, 2023b.

Mitchell Wortsman, Gabriel Ilharco, Samir Ya Gadre, Rebecca Roelofs, Raphael Gontijo-Lopes, Ari S Morcos, Hongseok Namkoong, Ali Farhadi, Yair Carmon, Simon Kornblith, et al. Model soups: averaging weights of multiple fine-tuned models improves accuracy without increasing inference time. In *International conference on machine learning*, pp. 23965–23998. PMLR, 2022.

Robert Wu and Vardan Papyan. Linguistic collapse: Neural collapse in (large) language models. *arXiv preprint arXiv:2405.17767*, 2024.

Enneng Yang, Zhenyi Wang, Li Shen, Shiwei Liu, Guibing Guo, Xingwei Wang, and Dacheng Tao. Adamerging: Adaptive model merging for multi-task learning. *arXiv preprint arXiv:2310.02575*, 2023.

Sihyun Yu, Sangkyung Kwak, Huiwon Jang, Jongheon Jeong, Jonathan Huang, Jinwoo Shin, and Saining Xie. Representation alignment for generation: Training diffusion transformers is easier than you think. *arXiv preprint arXiv:2410.06940*, 2024.

Li Yuan, Francis EH Tay, Guilin Li, Tao Wang, and Jiashi Feng. Revisiting knowledge distillation via label smoothing regularization. In *Proceedings of the IEEE/CVF conference on computer vision and pattern recognition*, pp. 3903–3911, 2020.

Rowan Zellers, Ari Holtzman, Yonatan Bisk, Ali Farhadi, and Yejin Choi. Hellaswag: Can a machine really finish your sentence? In *Proceedings of the 57th Annual Meeting of the Association for Computational Linguistics*, 2019.

Linfeng Zhang, Jiebo Song, Anni Gao, Jingwei Chen, Chenglong Bao, and Kaisheng Ma. Be your own teacher: Improve the performance of convolutional neural networks via self distillation. In *Proceedings of the IEEE/CVF international conference on computer vision*, pp. 3713–3722, 2019.

Minjia Zhang and Yuxiong He. Accelerating training of transformer-based language models with progressive layer dropping. *Advances in neural information processing systems*, 33:14011–14023, 2020.

Ying Zhang, Tao Xiang, Timothy M Hospedales, and Huchuan Lu. Deep mutual learning. In *Proceedings of the IEEE conference on computer vision and pattern recognition*, pp. 4320–4328, 2018.

Yue Zhou, Chenlu Guo, Xu Wang, Yi Chang, and Yuan Wu. A survey on data augmentation in large model era. *arXiv preprint arXiv:2401.15422*, 2024.

Yuyan Zhou, Liang Song, Bingning Wang, and Weipeng Chen. MetaGPT: Merging Large Language Models Using Model Exclusive Task Arithmetic. *arXiv e-prints*, art. arXiv:2406.11385, June 2024.

Zeyuan Allen Zhu and Yuanzhi Li. Physics of language models: Part 3.1, knowledge storage and extraction. *arXiv preprint arXiv:2309.14316*, 2023.

A PROOF OF THEOREM 1

In this section, we provide a detailed proof of Theorem 1. For any proportionality factor $\alpha \in (0, 1)$, the squared Euclidean distance between the pre-trained model parameters $\boldsymbol{\theta}_i$ and the target parameters $\boldsymbol{\theta}^\star$ is bounded probabilistically as follows:

$$\Pr\left(\|\boldsymbol{\theta}_i - \boldsymbol{\theta}^\star\|_2^2 \leq \alpha \|\boldsymbol{\theta}_{\text{rand}} - \boldsymbol{\theta}^\star\|_2^2\right) \geq 1 - O\left(\frac{\tau^2 + \beta}{\alpha}\right),$$

where $\boldsymbol{\theta}_{\text{rand}}$ represents the randomly initialized model parameters, $\boldsymbol{\theta}_i$ denotes the parameters of the i-th pre-trained model, and $\boldsymbol{\theta}^\star$ is the optimal parameters for the target dataset distribution $D^\star$. The terms τ and β reflect the variance of the mean difference and the upper bound on the perturbation variance, respectively.

Proof. We analyze the convergence behavior of gradient descent when initialized at $\boldsymbol{\theta}_i$ compared to random initialization. Here, $\boldsymbol{\theta}$ represents the model parameters, and $\boldsymbol{\theta}_i$ denotes the parameters of the i-th pre-trained model.

Assumption 1 (Data Mean Distribution) . *The mean of the i-th pre-training dataset distribution D_i is denoted as μ_i, which follows a normal distribution centered around the mean of the target dataset distribution $D^\star$, represented by $\mu^\star$, with variance τ^2:*

$$\mu_i \sim \mathcal{N}(\mu^\star, \tau^2).$$

Assumption 2 (Data Variance Distribution) . *The variance of the i-th pre-training dataset distribution D_i, denoted as σ_i^2, is perturbed from the variance of the target dataset distribution $D^\star$, denoted as $\sigma^{\star 2}$, by a small noise term δ:*

$$\sigma_i^2 = \sigma^{\star 2} + \delta,$$

where δ satisfies $\mathbb{E}[\delta] = 0$ and Var$(\delta) \leq \beta$.

Assumption 3 (Random Initialization Distribution) . *The randomly initialized model parameters $\boldsymbol{\theta}_{rand}$ are drawn from a standard normal distribution:*

$$\boldsymbol{\theta}_{rand} \sim \mathcal{N}(0, \mathbf{I}),$$

where $\mathbf{I}$ is the identity matrix, indicating independent parameters with unit variance.

Assumption 4 (Relationship Between Parameters and Data Features) . *The model parameters $\boldsymbol{\theta}_i$ are a deterministic function of the dataset features (μ_i, σ_i^2):*

$$\boldsymbol{\theta}_i = \boldsymbol{f}(\mu_i, \sigma_i^2),$$

where $\boldsymbol{f}$ is a Lipschitz continuous function. That is, there exists a constant $L > 0$ such that for any two feature pairs (μ_1, σ_1^2) and (μ_2, σ_2^2), the following condition holds:

$$\left\|\boldsymbol{f}(\mu_1, \sigma_1^2) - \boldsymbol{f}(\mu_2, \sigma_2^2)\right\|_2 \leq L\sqrt{(\mu_1 - \mu_2)^2 + (\sigma_1^2 - \sigma_2^2)^2}.$$

We begin by applying the Markov inequality to control the probabilistic bound on the distance between the pre-trained model parameters $\boldsymbol{\theta}_i$ and the target parameters $\boldsymbol{\theta}^\star$.

Step 1: Bounding the Expected Distance Let $X = \|\boldsymbol{\theta}_i - \boldsymbol{\theta}^\star\|_2^2$ represent the squared distance between $\boldsymbol{\theta}_i$ and $\boldsymbol{\theta}^\star$. Under the Lipschitz continuity assumption from Assumptions 1 and 2, we have:

$$\mathbb{E}[X] \leq L^2(\tau^2 + \beta),$$

where L is the Lipschitz constant, τ^2 is the variance of the mean difference, and β is the upper bound on the variance of the perturbation term.

Step 2: Application of Markov Inequality Let $Y = \|\boldsymbol{\theta}_{\text{rand}} - \boldsymbol{\theta}^\star\|_2^2$ represent the squared distance between the randomly initialized parameters $\boldsymbol{\theta}_{\text{rand}}$ and $\boldsymbol{\theta}^\star$.

To control the probability that X exceeds αY, we apply the Markov inequality:

$$\mathbb{P}\left(X \geq \alpha Y\right) \leq \frac{\mathbb{E}[X]}{\alpha \mathbb{E}[Y]}.$$

We compute $\mathbb{E}[Y]$ as follows.

Since $\boldsymbol{\theta}_{\text{rand}} \sim \mathcal{N}(0, \mathbf{I})$ as stated in Assumption 3, each component $(\boldsymbol{\theta}_{\text{rand}})_i$ is independently and identically distributed as $\mathcal{N}(0, 1)$. Therefore,

$$\mathbb{E}[Y] = \mathbb{E}\left[\|\boldsymbol{\theta}_{\text{rand}} - \boldsymbol{\theta}^\star\|_2^2\right] = \mathbb{E}\left[\|\boldsymbol{\theta}_{\text{rand}}\|_2^2 - 2(\boldsymbol{\theta}_{\text{rand}})^\top \boldsymbol{\theta}^\star + \|\boldsymbol{\theta}^\star\|_2^2\right].$$

Since $\mathbb{E}[\boldsymbol{\theta}_{\text{rand}}] = \mathbf{0}$ and $\boldsymbol{\theta}^\star$ is a constant vector, we have:

$$\mathbb{E}\left[(\boldsymbol{\theta}_{\text{rand}})^\top \boldsymbol{\theta}^\star\right] = \sum_{i=1}^{d} \mathbb{E}\left[(\boldsymbol{\theta}_{\text{rand}})_i\right] (\boldsymbol{\theta}^\star)_i = 0.$$

Additionally, since each $(\boldsymbol{\theta}_{\text{rand}})_i$ has variance 1, we find:

$$\mathbb{E}\left[\|\boldsymbol{\theta}_{\text{rand}}\|_2^2\right] = \sum_{i=1}^{d} \mathbb{E}\left[(\boldsymbol{\theta}_{\text{rand}})_i^2\right] = \sum_{i=1}^{d} \left(\text{Var}\left[(\boldsymbol{\theta}_{\text{rand}})_i\right] + \left(\mathbb{E}\left[(\boldsymbol{\theta}_{\text{rand}})_i\right]\right)^2\right) = d.$$

Therefore, we have:

$$\mathbb{E}[Y] = d + \|\boldsymbol{\theta}^\star\|_2^2,$$

where d is the dimensionality of the parameter space.

Substituting the bounds on $\mathbb{E}[X]$ and $\mathbb{E}[Y]$, we get:

$$\mathbb{P}\left(\|\boldsymbol{\theta}_i - \boldsymbol{\theta}^\star\|_2^2 \geq \alpha \|\boldsymbol{\theta}_{\text{rand}} - \boldsymbol{\theta}^\star\|_2^2\right) \leq \frac{L^2(\tau^2 + \beta)}{\alpha(d + \|\boldsymbol{\theta}^\star\|_2^2)}.$$

Step 3: Final Probabilistic Bound Taking the complement of the above inequality, we have:

$$\mathbb{P}\left(\|\boldsymbol{\theta}_i - \boldsymbol{\theta}^\star\|_2^2 \leq \alpha \|\boldsymbol{\theta}_{\text{rand}} - \boldsymbol{\theta}^\star\|_2^2\right) \geq 1 - \frac{L^2(\tau^2 + \beta)}{\alpha(d + \|\boldsymbol{\theta}^\star\|_2^2)}.$$

This yields the desired result:

$$\mathbb{P}\left(\|\boldsymbol{\theta}_i - \boldsymbol{\theta}^\star\|_2^2 \leq \alpha \|\boldsymbol{\theta}_{\text{rand}} - \boldsymbol{\theta}^\star\|_2^2\right) \geq 1 - O\left(\frac{\tau^2 + \beta}{\alpha}\right).$$

□

B Proof of Theorem 2

In this section, we provide a detailed proof of Theorem 2. The theorem establishes that initializing gradient descent with the proximal parameter $\boldsymbol{\theta}^P$, which is a weighted combination of transformed pre-trained model parameters, leads to faster convergence towards the optimal parameter $\boldsymbol{\theta}^\star$ compared to random initialization.

We make the following assumptions about the loss function $\mathcal{J}_D(\boldsymbol{\theta})$:

Assumption 5 (Loss Function Properties) . *The loss function $\mathcal{J}_D(\boldsymbol{\theta}) = \mathbb{E}_{(\mathbf{x},y)\sim D}[\ell(\phi_{\boldsymbol{\theta}}(\mathbf{x}), y)]$ is differentiable, convex, and satisfies:*

(a) ***L-smoothness:*** *There exists a constant $L > 0$ such that for all $\boldsymbol{\theta}, \boldsymbol{\theta}' \in \mathbb{R}^d$,*

$$\|\nabla \mathcal{J}_D(\boldsymbol{\theta}) - \nabla \mathcal{J}_D(\boldsymbol{\theta}')\|_2 \leq L\|\boldsymbol{\theta} - \boldsymbol{\theta}'\|_2.$$

(b) ***Strong Convexity:*** *There exists a constant $\mu > 0$ such that for all $\boldsymbol{\theta}, \boldsymbol{\theta}' \in \mathbb{R}^d$,*

$$\mathcal{J}_D(\boldsymbol{\theta}') \geq \mathcal{J}_D(\boldsymbol{\theta}) + \langle \nabla \mathcal{J}_D(\boldsymbol{\theta}), \boldsymbol{\theta}' - \boldsymbol{\theta} \rangle + \frac{\mu}{2}\|\boldsymbol{\theta}' - \boldsymbol{\theta}\|_2^2.$$

Proof. **Step 1: Gradient Descent Convergence Rate**

Under Assumption 5, specifically the L-smoothness and strong convexity of $\mathcal{J}_D(\boldsymbol{\theta})$, gradient descent with a fixed learning rate $\eta \in \left(0, \frac{1}{L}\right)$ satisfies the following convergence rate:

$$\mathcal{J}_D(\boldsymbol{\theta}^{(T)}) - \mathcal{J}_D(\boldsymbol{\theta}^\star) \leq (1 - \eta\mu)^T \left(\mathcal{J}_D(\boldsymbol{\theta}^{(0)}) - \mathcal{J}_D(\boldsymbol{\theta}^\star)\right).$$

This result leverages the properties of gradient descent on strongly convex and smooth functions.

Starting from the gradient descent update rule:

$$\boldsymbol{\theta}^{(t+1)} = \boldsymbol{\theta}^{(t)} - \eta \nabla \mathcal{J}_D(\boldsymbol{\theta}^{(t)}),$$

and applying the L-smoothness of Assumption 5, we have:

$$\mathcal{J}_D(\boldsymbol{\theta}^{(t+1)}) \leq \mathcal{J}_D(\boldsymbol{\theta}^{(t)}) + \langle \nabla \mathcal{J}_D(\boldsymbol{\theta}^{(t)}), \boldsymbol{\theta}^{(t+1)} - \boldsymbol{\theta}^{(t)} \rangle + \frac{L}{2} \|\boldsymbol{\theta}^{(t+1)} - \boldsymbol{\theta}^{(t)}\|_2^2.$$

Substituting the update rule into the inequality:

$$\begin{aligned}\mathcal{J}_D(\boldsymbol{\theta}^{(t+1)}) &\leq \mathcal{J}_D(\boldsymbol{\theta}^{(t)}) - \eta \|\nabla \mathcal{J}_D(\boldsymbol{\theta}^{(t)})\|_2^2 + \frac{L}{2}\eta^2 \|\nabla \mathcal{J}_D(\boldsymbol{\theta}^{(t)})\|_2^2 \\ &= \mathcal{J}_D(\boldsymbol{\theta}^{(t)}) - \eta \left(1 - \frac{L\eta}{2}\right) \|\nabla \mathcal{J}_D(\boldsymbol{\theta}^{(t)})\|_2^2.\end{aligned}$$

Next, we claim the following inequality:

$$\|\nabla \mathcal{J}_D(\boldsymbol{\theta}^{(t)})\|_2^2 \geq 2\mu \left(\mathcal{J}_D(\boldsymbol{\theta}^{(t)}) - \mathcal{J}_D(\boldsymbol{\theta}^\star)\right).$$

Proof of the Claim:

Under the strong convexity of Assumption 5, we have:

$$\mathcal{J}_D(\boldsymbol{\theta}^\star) \geq \mathcal{J}_D(\boldsymbol{\theta}^{(t)}) + \langle \nabla \mathcal{J}_D(\boldsymbol{\theta}^{(t)}), \boldsymbol{\theta}^\star - \boldsymbol{\theta}^{(t)} \rangle + \frac{\mu}{2} \|\boldsymbol{\theta}^\star - \boldsymbol{\theta}^{(t)}\|_2^2.$$

Rearranging terms gives:

$$\mathcal{J}_D(\boldsymbol{\theta}^{(t)}) \leq \mathcal{J}_D(\boldsymbol{\theta}^\star) + \langle \nabla \mathcal{J}_D(\boldsymbol{\theta}^{(t)}), \boldsymbol{\theta}^{(t)} - \boldsymbol{\theta}^\star \rangle - \frac{\mu}{2} \|\boldsymbol{\theta}^{(t)} - \boldsymbol{\theta}^\star\|_2^2.$$

By the Cauchy-Schwarz inequality:

$$\langle \nabla \mathcal{J}_D(\boldsymbol{\theta}^{(t)}), \boldsymbol{\theta}^{(t)} - \boldsymbol{\theta}^\star \rangle \leq \|\nabla \mathcal{J}_D(\boldsymbol{\theta}^{(t)})\|_2 \cdot \|\boldsymbol{\theta}^{(t)} - \boldsymbol{\theta}^\star\|_2.$$

Substituting this into the previous inequality:

$$\mathcal{J}_D(\boldsymbol{\theta}^{(t)}) \leq \mathcal{J}_D(\boldsymbol{\theta}^\star) + \|\nabla \mathcal{J}_D(\boldsymbol{\theta}^{(t)})\|_2 \cdot \|\boldsymbol{\theta}^{(t)} - \boldsymbol{\theta}^\star\|_2 - \frac{\mu}{2} \|\boldsymbol{\theta}^{(t)} - \boldsymbol{\theta}^\star\|_2^2.$$

Let $t = \|\boldsymbol{\theta}^{(t)} - \boldsymbol{\theta}^\star\|_2$. Then:

$$\mathcal{J}_D(\boldsymbol{\theta}^{(t)}) - \mathcal{J}_D(\boldsymbol{\theta}^\star) \leq \|\nabla \mathcal{J}_D(\boldsymbol{\theta}^{(t)})\|_2 \cdot t - \frac{\mu}{2} t^2.$$

According to the properties of quadratic functions, the maximum of the right-hand side occurs at:

$$t = \frac{\|\nabla \mathcal{J}_D(\boldsymbol{\theta})\|_2}{\mu}.$$

Substituting this value back, we have:

$$\mathcal{J}_D(\boldsymbol{\theta}) - \mathcal{J}_D(\boldsymbol{\theta}^\star) \leq \frac{\|\nabla \mathcal{J}_D(\boldsymbol{\theta})\|_2^2}{2\mu}.$$

Rearranging terms gives:

$$\|\nabla \mathcal{J}_D(\boldsymbol{\theta})\|_2^2 \geq 2\mu \left(\mathcal{J}_D(\boldsymbol{\theta}) - \mathcal{J}_D(\boldsymbol{\theta}^\star)\right).$$

This completes the proof of the claim.

Substituting this into the previous inequality:

$$\mathcal{J}_D(\boldsymbol{\theta}^{(t+1)}) - \mathcal{J}_D(\boldsymbol{\theta}^\star) \leq \mathcal{J}_D(\boldsymbol{\theta}^{(t)}) - \mathcal{J}_D(\boldsymbol{\theta}^\star) - 2\mu\eta\left(1 - \frac{L\eta}{2}\right)\left(\mathcal{J}_D(\boldsymbol{\theta}^{(t)}) - \mathcal{J}_D(\boldsymbol{\theta}^\star)\right)$$
$$= \left(1 - 2\mu\eta\left(1 - \frac{L\eta}{2}\right)\right)\left(\mathcal{J}_D(\boldsymbol{\theta}^{(t)}) - \mathcal{J}_D(\boldsymbol{\theta}^\star)\right).$$

Since $\eta \in \left(0, \frac{1}{L}\right)$, we have:

$$1 - 2\mu\eta\left(1 - \frac{L\eta}{2}\right) \leq 1 - \mu\eta.$$

Thus, we obtain:

$$\mathcal{J}_D(\boldsymbol{\theta}^{(t+1)}) - \mathcal{J}_D(\boldsymbol{\theta}^\star) \leq (1 - \mu\eta)\left(\mathcal{J}_D(\boldsymbol{\theta}^{(t)}) - \mathcal{J}_D(\boldsymbol{\theta}^\star)\right).$$

By recursively applying this inequality, we derive the convergence rate after T iterations:

$$\mathcal{J}_D(\boldsymbol{\theta}^{(T)}) - \mathcal{J}_D(\boldsymbol{\theta}^\star) \leq (1 - \mu\eta)^T\left(\mathcal{J}_D(\boldsymbol{\theta}^{(0)}) - \mathcal{J}_D(\boldsymbol{\theta}^\star)\right).$$

This demonstrates that the suboptimality decreases exponentially with the number of iterations T, confirming the linear convergence rate of gradient descent under the given assumptions.

Step 2: Bounding the Initial Suboptimality

We aim to bound the initial suboptimality $\mathcal{J}_D(\boldsymbol{\theta}^P) - \mathcal{J}_D(\boldsymbol{\theta}^\star)$. Utilizing the smoothness of $\mathcal{J}_D(\boldsymbol{\theta})$, we have for any $\boldsymbol{\theta} \in \mathbb{R}^d$:

$$\mathcal{J}_D(\boldsymbol{\theta}) \leq \mathcal{J}_D(\boldsymbol{\theta}^\star) + \langle \nabla\mathcal{J}_D(\boldsymbol{\theta}^\star), \boldsymbol{\theta} - \boldsymbol{\theta}^\star\rangle + \frac{L}{2}\|\boldsymbol{\theta} - \boldsymbol{\theta}^\star\|_2^2.$$

Since $\boldsymbol{\theta}^\star$ is the minimizer of $\mathcal{J}_D(\boldsymbol{\theta})$, it satisfies $\nabla\mathcal{J}_D(\boldsymbol{\theta}^\star) = 0$. Therefore, the inequality simplifies to:

$$\mathcal{J}_D(\boldsymbol{\theta}) - \mathcal{J}_D(\boldsymbol{\theta}^\star) \leq \frac{L}{2}\|\boldsymbol{\theta} - \boldsymbol{\theta}^\star\|_2^2.$$

Setting $\boldsymbol{\theta} = \boldsymbol{\theta}^P$, we obtain:

$$\mathcal{J}_D(\boldsymbol{\theta}^P) - \mathcal{J}_D(\boldsymbol{\theta}^\star) \leq \frac{L}{2}\|\boldsymbol{\theta}^P - \boldsymbol{\theta}^\star\|_2^2.$$

Step 3: Combining the Results

Substituting the bound on the initial suboptimality into the convergence rate from Step 1, we get:

$$\mathcal{J}_D(\boldsymbol{\theta}^{(T)}) - \mathcal{J}_D(\boldsymbol{\theta}^\star) \leq (1 - \eta\mu)^T\left(\frac{L}{2}\|\boldsymbol{\theta}^P - \boldsymbol{\theta}^\star\|_2^2\right).$$

This inequality demonstrates that the suboptimality after T iterations decays exponentially with rate $(1 - \eta\mu)^T$, scaled by the initial suboptimality $\frac{L}{2}\|\boldsymbol{\theta}^P - \boldsymbol{\theta}^\star\|_2^2$. □

C THE CONVERGENCE ADVANTAGE WITH PROXIMAL PARAMETER INITIALIZATION

We will demonstrate why proximal parameter initialization ($\boldsymbol{\theta}^P$) is likely to lead to faster convergence compared to random initialization ($\boldsymbol{\theta}_{\text{rand}}$) in gradient descent. We provide both an intuitive explanation and a detailed proof.

C.1 Intuitive Explanation

We recall Theorem 2, which establishes a relationship between the suboptimality of the loss function and the distance of the parameters from the optimal parameter $\boldsymbol{\theta}^\star$:

$$\mathcal{J}_D(\boldsymbol{\theta}^{(T)}) - \mathcal{J}_D(\boldsymbol{\theta}^\star) \leq (1-\eta\mu)^T \left(\mathcal{J}_D(\boldsymbol{\theta}^P) - \mathcal{J}_D(\boldsymbol{\theta}^\star)\right),$$

where $\mathcal{J}(\boldsymbol{\theta}^P) - \mathcal{J}_D(\boldsymbol{\theta}^\star) \leq \frac{L}{2}\left\|\boldsymbol{\theta}^P - \boldsymbol{\theta}^\star\right\|_2^2$. From this, we observe that when $\boldsymbol{\theta}^{(0)} = \boldsymbol{\theta}^P$, the difference in the loss function is controlled by the parameter distance $\left\|\boldsymbol{\theta}^P - \boldsymbol{\theta}^\star\right\|_2^2$. From the proof in Step 2 of Appendix B, we observe that this conclusion does not depend on the specific choice of $\boldsymbol{\theta}^P$. Therefore, when $\boldsymbol{\theta}^{(0)} = \boldsymbol{\theta}_{\text{rand}}$, the conclusion still holds. Hence, when analyzing the convergence of the loss function, we only need to compare the initial distances of the parameters.

Theorem 1 provides a probabilistic bound on the parameter distances:

$$\Pr\left(\|\boldsymbol{\theta}_i - \boldsymbol{\theta}^\star\|_2^2 \leq \alpha\|\boldsymbol{\theta}_{\text{rand}} - \boldsymbol{\theta}^\star\|_2^2\right) \geq 1 - O\left(\frac{\tau^2+\beta}{\alpha}\right).$$

This indicates that pre-trained model parameters $\boldsymbol{\theta}_i$ are, with high probability, closer to the optimal parameter $\boldsymbol{\theta}^\star$ than randomly initialized parameters $\boldsymbol{\theta}_{\text{rand}}$. Since the proximal parameter $\boldsymbol{\theta}^P = \sum_{i=1}^n \gamma_i^\star \boldsymbol{\theta}_i$, $\boldsymbol{\theta}^P$ is also likely to be closer to $\boldsymbol{\theta}^\star$ than $\boldsymbol{\theta}_{\text{rand}}$, ensuring faster convergence.

C.2 Detailed Proof

Proof. We aim to show that proximal parameter initialization $\boldsymbol{\theta}^P$ is likely to lead to faster convergence compared to random initialization $\boldsymbol{\theta}_{\text{rand}}$. This proof builds upon the assumptions of smoothness and strong convexity (see Assumptions 5).

Step 1: Bounding the Parameter Distances

From Theorem 1, we know that pre-trained parameters $\boldsymbol{\theta}_i$ are, with high probability, closer to the optimal parameter $\boldsymbol{\theta}^\star$ than randomly initialized parameters $\boldsymbol{\theta}_{\text{rand}}$. Specifically:

$$\Pr\left(\|\boldsymbol{\theta}_i - \boldsymbol{\theta}^\star\|_2^2 \leq \alpha\|\boldsymbol{\theta}_{\text{rand}} - \boldsymbol{\theta}^\star\|_2^2\right) \geq 1 - O\left(\frac{\tau^2+\beta}{\alpha}\right),$$

where α is a positive scalar.

To select α, we choose $\alpha = \frac{\mu}{2L}$, which ensures $\alpha \in (0,1)$ since $\mu < L$ for a strongly convex and smooth function. With this choice of α, the distance between pre-trained parameters and the optimal parameter $\boldsymbol{\theta}^\star$ satisfies, with high probability:

$$\|\boldsymbol{\theta}_i - \boldsymbol{\theta}^\star\|_2^2 \leq \alpha\|\boldsymbol{\theta}_{\text{rand}} - \boldsymbol{\theta}^\star\|_2^2.$$

We now bound the distance between the proximal parameter $\boldsymbol{\theta}^P$ and $\boldsymbol{\theta}^\star$. Since $\boldsymbol{\theta}^P = \sum_{i=1}^n \gamma_i^\star \boldsymbol{\theta}_i$, where $\gamma_i^\star$ are non-negative weights summing to 1, by convexity of the squared norm:

$$\|\boldsymbol{\theta}^P - \boldsymbol{\theta}^\star\|_2^2 = \left\|\sum_{i=1}^n \gamma_i^\star(\boldsymbol{\theta}_i - \boldsymbol{\theta}^\star)\right\|_2^2 \leq \left(\sum_{i=1}^n \gamma_i^\star\|\boldsymbol{\theta}_i - \boldsymbol{\theta}^\star\|_2\right)^2.$$

Substituting the bound $\|\boldsymbol{\theta}_i - \boldsymbol{\theta}^\star\|_2 \leq \sqrt{\alpha}\|\boldsymbol{\theta}_{\text{rand}} - \boldsymbol{\theta}^\star\|_2$, we obtain, with high probability:

$$\|\boldsymbol{\theta}^P - \boldsymbol{\theta}^\star\|_2^2 \leq \alpha\|\boldsymbol{\theta}_{\text{rand}} - \boldsymbol{\theta}^\star\|_2^2.$$

Step 2: Relating the Loss Functions Using the Parameter Bounds

Using the result of Theorem 2, we relate the proximal parameter distance to the suboptimality of the loss:

$$\mathcal{J}_D(\boldsymbol{\theta}^P) - \mathcal{J}_D(\boldsymbol{\theta}^\star) \leq \frac{L}{2}\|\boldsymbol{\theta}^P - \boldsymbol{\theta}^\star\|_2^2.$$

Substituting the bound on $\|\boldsymbol{\theta}^P - \boldsymbol{\theta}^\star\|_2^2$ from Step 1, we get, with high probability:

$$\mathcal{J}_D(\boldsymbol{\theta}^P) - \mathcal{J}_D(\boldsymbol{\theta}^\star) \leq \frac{L}{2}\alpha\|\boldsymbol{\theta}_{\text{rand}} - \boldsymbol{\theta}^\star\|_2^2.$$

For $\boldsymbol{\theta}_{\text{rand}}$, applying the strong convexity property, we can derive a lower bound for the loss function. We have the inequality:

$$\mathcal{J}_D(\boldsymbol{\theta}_{\text{rand}}) \geq \mathcal{J}_D(\boldsymbol{\theta}^\star) + \langle \nabla \mathcal{J}_D(\boldsymbol{\theta}^\star), \boldsymbol{\theta}_{\text{rand}} - \boldsymbol{\theta}^\star \rangle + \frac{\mu}{2}\|\boldsymbol{\theta}_{\text{rand}} - \boldsymbol{\theta}^\star\|_2^2.$$

Since $\boldsymbol{\theta}^\star$ is the optimal solution, we know that $\nabla \mathcal{J}_D(\boldsymbol{\theta}^\star) = 0$. Therefore, the inequality simplifies to:

$$\mathcal{J}_D(\boldsymbol{\theta}_{\text{rand}}) - \mathcal{J}_D(\boldsymbol{\theta}^\star) \geq \frac{\mu}{2}\|\boldsymbol{\theta}_{\text{rand}} - \boldsymbol{\theta}^\star\|_2^2.$$

Taking the ratio of the inequalities above, we have:

$$\rho = \frac{\mathcal{J}(\boldsymbol{\theta}^P) - \mathcal{J}_D(\boldsymbol{\theta}^\star)}{\mathcal{J}(\boldsymbol{\theta}_{\text{rand}}) - \mathcal{J}_D(\boldsymbol{\theta}^\star)} \leq \frac{L\alpha}{\mu} = \frac{L}{\mu} \cdot \frac{\mu}{2L} = \frac{1}{2}.$$

Therefore, we have:

$$\mathcal{J}(\boldsymbol{\theta}^P) - \mathcal{J}_D(\boldsymbol{\theta}^\star) \leq \frac{1}{2}\mathcal{J}(\boldsymbol{\theta}_{\text{rand}}) - \mathcal{J}_D(\boldsymbol{\theta}^\star).$$

It can be seen that when $\boldsymbol{\theta}^{(0)} = \boldsymbol{\theta}^P$, the upper bound of the loss function is smaller than that of random initialization with high probability. According to the result of Theorem 2:

$$\mathcal{J}_D(\boldsymbol{\theta}^{(T)}) - \mathcal{J}_D(\boldsymbol{\theta}^\star) \leq (1 - \eta\mu)^T \left(\mathcal{J}_D(\boldsymbol{\theta}^P) - \mathcal{J}_D(\boldsymbol{\theta}^\star)\right),$$

We observe that the advantage of the upper bound provided by proximal initialization will persist for a number of iterations. However, as T increases, this advantage cannot always be relied upon as a strong performance guarantee in later iterations. □

D Generalization Error Upper Bound

In the context of transfer learning, understanding how well a model trained on a pre-trained dataset generalizes to a target dataset is crucial. Let D_i and $D^\star$ denote the true data distributions of the pre-trained and target datasets, respectively. Since these distributions are generally unknown, we rely on labeled samples drawn from them to estimate the necessary quantities.

Assume we have labeled datasets from both the pre-trained and target datasets. For the pre-trained dataset, the sample is given as $U_i = \{(\mathbf{x}_{ij}, \mathbf{y}_{ij})\}_{j=1}^{n_i}$, where $(\mathbf{x}_{ij}, \mathbf{y}_{ij}) \sim D_i$. Similarly, for the target dataset, the sample is $U^\star = \{(\mathbf{x}_j^\star, \mathbf{y}_j^\star)\}_{j=1}^{n^\star}$, where $(\mathbf{x}_j^\star, \mathbf{y}_j^\star) \sim D^\star$. Our goal is to derive a computable upper bound on the generalization error of a hypothesis $\boldsymbol{\phi}$ from a hypothesis space $\mathcal{H}$ when applied to the target dataset.

The hypothesis space $\mathcal{H}$ consists of measurable functions mapping inputs $\mathbf{x}$ to outputs $\boldsymbol{\phi}(\mathbf{x})$. We use a loss function $\ell : \mathcal{Y} \times \mathcal{Y} \to [0, C]$, which is non-negative and bounded by a constant $C > 0$. This function measures the discrepancy between the model predictions and the true labels. We assume the samples in U_i and $U^\star$ are independently and identically distributed (i.i.d.) according to their respective distributions.

The empirical distribution $\hat{D}_{U_i}$ induced by the pre-trained dataset U_i is defined as:

$$\hat{D}_{U_i}(\mathbf{x}, \mathbf{y}) = \frac{1}{n_i}\sum_{j=1}^{n_i} \delta_{(\mathbf{x}_{ij}, \mathbf{y}_{ij})}(\mathbf{x}, \mathbf{y}),$$

where $\delta_{(\mathbf{x}_{ij}, \mathbf{y}_{ij})}(\mathbf{x}, \mathbf{y})$ is the Dirac delta function centered at $(\mathbf{x}_{ij}, \mathbf{y}_{ij})$. Similarly, the empirical distribution $\hat{D}_{U^\star}$ based on the target dataset $U^\star$ is defined as:

$$\hat{D}_{U^\star}(\mathbf{x}, \mathbf{y}) = \frac{1}{n^\star}\sum_{j=1}^{n^\star} \delta_{(\mathbf{x}_j^\star, \mathbf{y}_j^\star)}(\mathbf{x}, \mathbf{y}).$$

These empirical distributions approximate the true distributions D_i and $D^\star$ based on the available samples.

The empirical total variation distance between the distributions of the pre-trained dataset $\hat{D}_{U_i}$ and the target dataset $\hat{D}_{U^\star}$ is defined as:

$$\mathrm{D_{TV}}(\hat{D}_{U_i}, \hat{D}_{U^\star}) = \frac{1}{2} \sum_{(\mathbf{x},\mathbf{y}) \in \mathcal{X} \times \mathcal{Y}} \left| \hat{D}_{U_i}(\mathbf{x}, \mathbf{y}) - \hat{D}_{U^\star}(\mathbf{x}, \mathbf{y}) \right|,$$

where $\hat{D}_{U_i}$ and $\hat{D}_{U^\star}$ are the empirical distributions based on the samples U_i and $U^\star$, respectively. This distance quantifies the discrepancy between the pre-trained and target datasets.

Assumption 6 (Bounded Loss Function) . *The loss function ℓ satisfies:*

$$0 \leq \ell(\boldsymbol{\phi}(\mathbf{x}), \mathbf{y}) \leq C, \quad \forall \boldsymbol{\phi} \in \mathcal{H},\ \forall (\mathbf{x}, \mathbf{y}) \in \mathcal{X} \times \mathcal{Y}.$$

This boundedness ensures that the loss remains within a fixed range, facilitating uniform convergence.

Definition 2 (Empirical Rademacher Complexity) . *The empirical Rademacher complexity of the loss-composed hypothesis space $\mathcal{L} \circ \mathcal{H}$ on the pre-trained dataset U_i is defined as:*

$$\hat{\mathfrak{R}}_{U_i}(\mathcal{L} \circ \mathcal{H}) = \mathbb{E}_{\boldsymbol{\sigma}} \left[\sup_{\boldsymbol{\phi} \in \mathcal{H}} \frac{1}{n_i} \sum_{j=1}^{n_i} \sigma_j \ell(\boldsymbol{\phi}(\mathbf{x}_{ij}), \mathbf{y}_{ij}) \right],$$

where $\boldsymbol{\sigma} = (\sigma_1, \ldots, \sigma_{n_i})$ are independent Rademacher variables taking values ± 1 with equal probability. This complexity measure captures the richness of the hypothesis space relative to the data.

Lemma 1 (Empirical Rademacher Complexity Upper Bound) . *For any $\boldsymbol{\phi} \in \mathcal{H}$, with probability at least $1 - \delta$, the following inequality holds:*

$$\mathcal{J}_{D_i}(\boldsymbol{\phi}) \leq \hat{\mathcal{J}}_{DU_i}(\boldsymbol{\phi}) + 2\hat{\mathfrak{R}}_{U_i}(\mathcal{L} \circ \mathcal{H}) + 3C\sqrt{\frac{\ln(2/\delta)}{2n_i}},$$

where $\mathcal{J}_{D_i}(\boldsymbol{\phi}) = \mathbb{E}_{(\mathbf{x},\mathbf{y}) \sim D_i}[\ell(\boldsymbol{\phi}(\mathbf{x}), \mathbf{y})]$ is the true risk on the pre-trained dataset. $\hat{\mathcal{J}}_{DU_i}(\boldsymbol{\phi}) = \frac{1}{n_i} \sum_{j=1}^{n_i} \ell(\boldsymbol{\phi}(\mathbf{x}_{ij}), \mathbf{y}_{ij})$ is the empirical risk on the pre-trained dataset U_i, which is an estimate of the true risk based on the sample data.

Theorem 4 (Generalization Error Upper Bound) . *Under the above assumptions, for any hypothesis $\boldsymbol{\phi}_{\boldsymbol{\theta}} \in \mathcal{H}$, with probability at least $1 - \delta$, the following inequality holds:*

$$\mathcal{J}_{D^\star}(\boldsymbol{\phi}_{\boldsymbol{\theta}}) \leq \hat{\mathcal{J}}_{U_i}(\boldsymbol{\phi}_{\boldsymbol{\theta}}) + 2C \cdot \mathrm{D_{TV}}(\hat{D}_{U_i}, \hat{D}_{U^\star}) + 2\hat{\mathfrak{R}}_{U_i}(\mathcal{H}) + 3C\sqrt{\frac{\ln(4/\delta)}{2n_i}} + \lambda,$$

where $\hat{\mathcal{J}}_{U_i}(\boldsymbol{\phi}_{\boldsymbol{\theta}})$ is the empirical expected loss, C is a constant bound, $\hat{\mathfrak{R}}_{U_i}(\mathcal{H})$ is the empirical Rademacher complexity of $\mathcal{H}$, and n_i is the size of the dataset U_i. Finally, $\lambda = \inf_{\boldsymbol{\phi}' \in \mathcal{H}} \left[\mathcal{J}_{D_i}(\boldsymbol{\phi}') + \mathcal{J}_{D^\star}(\boldsymbol{\phi}') \right]$, represents the minimal combined risk over $\mathcal{H}$.

Proof. We begin by expressing the target domain risk $\mathcal{J}_{D^\star}(\boldsymbol{\phi})$ in terms of the source domain risk:

$$\mathcal{J}_{D^\star}(\boldsymbol{\phi}) = \mathcal{J}_{D_i}(\boldsymbol{\phi}) + \left[\mathcal{J}_{D^\star}(\boldsymbol{\phi}) - \mathcal{J}_{D_i}(\boldsymbol{\phi}) \right].$$

Step 1: Bounding the Risk Difference Using Total Variation Distance

The difference $\mathcal{J}_{D^\star}(\boldsymbol{\phi}) - \mathcal{J}_{D_i}(\boldsymbol{\phi})$ can be bounded using the total variation distance and the boundedness of the loss function:

$$\begin{aligned}
|\mathcal{J}_{D^\star}(\boldsymbol{\phi}) - \mathcal{J}_{D_i}(\boldsymbol{\phi})| &= \left|\mathbb{E}_{(\mathbf{x},\mathbf{y})\sim D^\star}[\ell(\boldsymbol{\phi}(\mathbf{x}),\mathbf{y})] - \mathbb{E}_{(\mathbf{x},\mathbf{y})\sim D_i}[\ell(\boldsymbol{\phi}(\mathbf{x}),\mathbf{y})]\right| \\
&= \left|\int_{\mathcal{X}\times\mathcal{Y}} \ell(\boldsymbol{\phi}(\mathbf{x}),\mathbf{y})\left[dD^\star(\mathbf{x},\mathbf{y}) - dD_i(\mathbf{x},\mathbf{y})\right]\right| \\
&\leq \int_{\mathcal{X}\times\mathcal{Y}} |\ell(\boldsymbol{\phi}(\mathbf{x}),\mathbf{y})|\,|dD^\star(\mathbf{x},\mathbf{y}) - dD_i(\mathbf{x},\mathbf{y})| \\
&\leq C\cdot\int_{\mathcal{X}\times\mathcal{Y}} |dD^\star(\mathbf{x},\mathbf{y}) - dD_i(\mathbf{x},\mathbf{y})| \\
&= 2C\cdot \mathrm{D}_{\mathrm{TV}}(D_i, D^\star).
\end{aligned}$$

Therefore, we have:

$$\mathcal{J}_{D^\star}(\boldsymbol{\phi}) \leq \mathcal{J}_{D_i}(\boldsymbol{\phi}) + 2C\cdot \mathrm{D}_{\mathrm{TV}}(D_i, D^\star).$$

Step 2: Approximating the Total Variation Distance

Since D_i and $D^\star$ are unknown, we approximate $\mathrm{D}_{\mathrm{TV}}(D_i, D^\star)$ using the empirical distributions $\hat{D}_{U_i}$ and $\hat{D}_{U^\star}$. However, we must account for the estimation error due to finite sample sizes.

Let ε be the error term such that:

$$\mathrm{D}_{\mathrm{TV}}(D_i, D^\star) \leq \mathrm{D}_{\mathrm{TV}}(\hat{D}_{U_i}, \hat{D}_{U^\star}) + \mathrm{D}_{\mathrm{TV}}(D_i, \hat{D}_{U_i}) + \mathrm{D}_{\mathrm{TV}}(D^\star, \hat{D}_{U^\star}).$$

Using concentration inequalities for total variation distance, we can bound $\mathrm{D}_{\mathrm{TV}}(D_i, \hat{D}_{U_i})$ and $\mathrm{D}_{\mathrm{TV}}(D^\star, \hat{D}_{U^\star})$. However, in high-dimensional spaces, these bounds may be loose.

For practical purposes, we proceed by accepting $\mathrm{D}_{\mathrm{TV}}(D_i, D^\star) \approx \mathrm{D}_{\mathrm{TV}}(\hat{D}_{U_i}, \hat{D}_{U^\star})$, acknowledging that the approximation improves with larger n_i and $n^\star$.

Thus, we have:

$$\mathcal{J}_{D^\star}(\boldsymbol{\phi}) \leq \mathcal{J}_{D_i}(\boldsymbol{\phi}) + 2C\cdot \mathrm{D}_{\mathrm{TV}}(\hat{D}_{U_i}, \hat{D}_{U^\star}) + 2C\cdot\varepsilon,$$

where ε represents the combined estimation error.

Step 3: Bounding the Source Domain Risk

Applying the lemma on empirical Rademacher complexity, with probability at least $1-\delta/2$:

$$\mathcal{J}_{D_i}(\boldsymbol{\phi}) \leq \hat{\mathcal{J}}_{DU_i}(\boldsymbol{\phi}) + 2\hat{\mathfrak{R}}_{U_i}(\mathcal{L}\circ\mathcal{H}) + 3C\sqrt{\frac{\ln(4/\delta)}{2n_i}}.$$

Step 4: Combining the Bounds

Using the union bound to ensure that both inequalities hold with probability at least $1-\delta$, we combine the results:

$$\mathcal{J}_{D^\star}(\boldsymbol{\phi}) \leq \hat{\mathcal{J}}_{DU_i}(\boldsymbol{\phi}) + 2C\cdot \mathrm{D}_{\mathrm{TV}}(\hat{D}_{U_i}, \hat{D}_{U^\star}) + 2\hat{\mathfrak{R}}_{U_i}(\mathcal{L}\circ\mathcal{H}) + 3C\sqrt{\frac{\ln(4/\delta)}{2n_i}} + 2C\cdot\varepsilon.$$

To account for the inherent discrepancy between D_i and $D^\star$ that cannot be mitigated by any hypothesis in $\mathcal{H}$, we introduce the irreducible error term:

$$\lambda = \inf_{\boldsymbol{\phi}'\in\mathcal{H}} \left[\mathcal{J}_{D_i}(\boldsymbol{\phi}') + \mathcal{J}_{D^\star}(\boldsymbol{\phi}')\right].$$

This term represents the minimal combined risk over $\mathcal{H}$ and reflects the best possible performance achievable across both domains.

Including λ in our bound, we have:

$$\mathcal{J}_{D^\star}(\boldsymbol{\phi}) \leq \hat{\mathcal{J}}_{DU_i}(\boldsymbol{\phi}) + 2C\cdot \mathrm{D}_{\mathrm{TV}}(\hat{D}_{U_i}, \hat{D}_{U^\star}) + 2\hat{\mathfrak{R}}_{U_i}(\mathcal{L}\circ\mathcal{H}) + 3C\sqrt{\frac{\ln(4/\delta)}{2n_i}} + \lambda + 2C\cdot\varepsilon.$$

Step 5: Relating Rademacher Complexities

According to Assumption 5, the loss function ℓ is Lipschitz continuous with constant L. Therefore:

$$\hat{\mathfrak{R}}_{U_i}(\mathcal{L} \circ \mathcal{H}) \leq L \cdot \hat{\mathfrak{R}}_{U_i}(\mathcal{H}).$$

Substituting back into our inequality:

$$\mathcal{J}_{D^\star}(\boldsymbol{\phi}) \leq \hat{\mathcal{J}}_{DU_i}(\boldsymbol{\phi}) + 2C \cdot \mathrm{D}_{\mathrm{TV}}(\hat{D}_{U_i}, \hat{D}_{U^\star}) + 2L\hat{\mathfrak{R}}_{U_i}(\mathcal{H}) + 3C\sqrt{\frac{\ln(4/\delta)}{2n_i}} + \lambda + 2C \cdot \varepsilon.$$

By acknowledging that ε diminishes with larger sample sizes and can be made arbitrarily small, we obtain the desired generalization error bound:

$$\mathcal{J}_{D^\star}(\boldsymbol{\phi}) \leq \hat{\mathcal{J}}_{DU_i}(\boldsymbol{\phi}) + 2C \cdot \mathrm{D}_{\mathrm{TV}}(\hat{D}_{U_i}, \hat{D}_{U^\star}) + 2L\hat{\mathfrak{R}}_{U_i}(\mathcal{H}) + 3C\sqrt{\frac{\ln(4/\delta)}{2n_i}} + \lambda.$$

□

E Proof of Theorem 3

We recall the statement of Theorem 3, which provides the optimal combination coefficients $\boldsymbol{\gamma}^\star = [\gamma_1^\star, \gamma_2^\star, \ldots, \gamma_n^\star]^\top$ for the proximal parameter $\boldsymbol{\theta}^{\mathrm{P}}$ in terms of the total variation distances between the distributions. The theorem can be divided into two cases:

(a) **Case $n = 2$:** When there are two pre-trained models, the optimal combination coefficients $\gamma_1^\star$ and $\gamma_2^\star$ that minimize the distance between the proximal parameter $\boldsymbol{\theta}^{\mathrm{P}}$ and the target parameter $\boldsymbol{\theta}^\star$ are given by:

$$\gamma_1^\star = \frac{\mathrm{D}_{\mathrm{TV}}(D_1, D^\star)^2 + \mathrm{D}_{\mathrm{TV}}(D_1, D_2)^2 - \mathrm{D}_{\mathrm{TV}}(D_2, D^\star)^2}{2\mathrm{D}_{\mathrm{TV}}(D_1, D_2)^2}, \quad \gamma_2^\star = 1 - \gamma_1^\star,$$

where $\mathrm{D}_{\mathrm{TV}}(D_i, D_j)$ denotes the total variation distance between distributions D_i and D_j. This solution is valid provided that $\gamma_1^\star, \gamma_2^\star \geq 0$.

(b) **Case $n > 2$:** For more than two pre-trained models, an explicit solution for the optimal combination coefficients $\boldsymbol{\gamma}^\star$ under the constraints $\gamma_i^\star \geq 0$ does not generally exist. However, if we assume $\gamma_i^\star > 0$ for all i, the coefficients can be determined as:

$$\boldsymbol{\gamma}^\star = \frac{\mathbf{H}^{-1}\mathbf{e}}{\mathbf{e}^\top \mathbf{H}^{-1}\mathbf{e}},$$

where:

$$H_{ij} = \mathrm{D}_{\mathrm{TV}}(D_i, D^\star)^2 + \mathrm{D}_{\mathrm{TV}}(D_j, D^\star)^2 - \mathrm{D}_{\mathrm{TV}}(D_i, D_j)^2,$$

and $\mathbf{e}$ is an n-dimensional vector with all entries equal to 1.

In the following steps, we provide a detailed proof of Theorem 3.

Proof. We begin by considering a binary classification problem using a linear model. For simplicity, assume the class labels $y \in \{-1, 1\}$ and input feature vectors $\boldsymbol{x} \in \mathbb{R}^d$. The objective is to predict the class label based on the input features.

In this proof, we employ Linear Discriminant Analysis (LDA). The goal of LDA is to find a linear decision boundary that separates the samples of different classes as effectively as possible. In LDA, the decision function is defined as:

$$f(\boldsymbol{x}) = \boldsymbol{\theta}^\top \boldsymbol{x} + b,$$

where the parameters $\boldsymbol{\theta}$ and b are determined by:

$$\boldsymbol{\theta} = \boldsymbol{\Sigma}^{-1}(\boldsymbol{\mu}^{(1)} - \boldsymbol{\mu}^{(-1)}), \quad b = -\frac{1}{2}(\boldsymbol{\mu}^{(1)} + \boldsymbol{\mu}^{(-1)})^\top \boldsymbol{\Sigma}^{-1}(\boldsymbol{\mu}^{(1)} - \boldsymbol{\mu}^{(-1)}) + \ln\left(\frac{P(y=1)}{P(y=-1)}\right).$$

Here, $\boldsymbol{\mu}^{(1)}$ and $\boldsymbol{\mu}^{(-1)}$ are the mean vectors of the features for classes $y = 1$ and $y = -1$, respectively, and $\boldsymbol{\Sigma}$ is the shared covariance matrix of the features.

Step 1: Assumptions

Assumption 7 (Class-Conditional Distribution) . *For each pre-trained dataset D_i and the target dataset $D^\star$, the input features $\boldsymbol{x}$ are conditionally Gaussian given the class label y:*

(a) For class $y = 1$:

$$\boldsymbol{x} \mid y = 1 \sim \mathcal{N}(\boldsymbol{\mu}_i^{(1)}, \boldsymbol{\Sigma}), \quad \boldsymbol{x} \mid y = 1 \sim \mathcal{N}(\boldsymbol{\mu}^{\star(1)}, \boldsymbol{\Sigma}),$$

where $\boldsymbol{\mu}_i^{(1)}$ and $\boldsymbol{\mu}^{\star(1)}$ are the mean vectors for class $y = 1$ in the pre-trained and target datasets, respectively.

(b) For class $y = -1$:

$$\boldsymbol{x} \mid y = -1 \sim \mathcal{N}(\boldsymbol{\mu}_i^{(-1)}, \boldsymbol{\Sigma}), \quad \boldsymbol{x} \mid y = -1 \sim \mathcal{N}(\boldsymbol{\mu}^{\star(-1)}, \boldsymbol{\Sigma}),$$

where $\boldsymbol{\mu}_i^{(-1)}$ and $\boldsymbol{\mu}^{\star(-1)}$ are the mean vectors for class $y = -1$.

(c) The covariance matrix $\boldsymbol{\Sigma}$ is shared across all datasets.

Assumption 8 (Covariance Matrix Properties) . *The class-conditional covariance matrix $\boldsymbol{\Sigma}$ satisfies:*

*(a) **Consistency:** The covariance matrices are the same for all pre-trained datasets D_i and the target dataset $D^\star$:*

$$\boldsymbol{\Sigma}_i = \boldsymbol{\Sigma}^\star = \boldsymbol{\Sigma}.$$

*(b) **Positive Definiteness:** The covariance matrix $\boldsymbol{\Sigma}$ is positive definite:*

$$\boldsymbol{\Sigma} \succ 0,$$

ensuring that $\boldsymbol{\Sigma}$ is invertible.

Step 2: Lemma in Linear Model

Lemma 2 (Parameter Distance and Total Variation) . *Under the above assumptions and given the linear model, the Euclidean distance between the parameters of the pre-trained models $\boldsymbol{\theta}_i$ and the target model $\boldsymbol{\theta}^\star$ is proportional to the total variation distance between their distributions:*

$$\|\boldsymbol{\theta}_i - \boldsymbol{\theta}^\star\| = C \cdot \mathrm{D}_{TV}(D_i, D^\star),$$

where

$$C = 2\sqrt{\frac{\tilde{\boldsymbol{\mu}}^\top \boldsymbol{\Lambda}^{-2} \tilde{\boldsymbol{\mu}}}{\tilde{\boldsymbol{\mu}}^\top \boldsymbol{\Lambda}^{-1} \tilde{\boldsymbol{\mu}}}} = 2\sqrt{\frac{\sum_{j=1}^d \frac{\tilde{\mu}_j^2}{\lambda_j^2}}{\sum_{j=1}^d \frac{\tilde{\mu}_j^2}{\lambda_j}}}$$

is a constant, which depends on the eigenvalues of the covariance matrix $\boldsymbol{\Sigma}$ and the components of the transformed mean difference.

Proof of Lemma 2. Given the LDA model, the parameters are related to the mean differences:

$$\boldsymbol{\theta}_i = \boldsymbol{\Sigma}^{-1}(\boldsymbol{\mu}_i^{(1)} - \boldsymbol{\mu}_i^{(-1)}), \quad \boldsymbol{\theta}^\star = \boldsymbol{\Sigma}^{-1}(\boldsymbol{\mu}^{\star(1)} - \boldsymbol{\mu}^{\star(-1)}).$$

The difference is:

$$\boldsymbol{\theta}_i - \boldsymbol{\theta}^\star = \boldsymbol{\Sigma}^{-1}(\boldsymbol{\mu}_i - \boldsymbol{\mu}^\star),$$

where $\boldsymbol{\mu}_i = \boldsymbol{\mu}_i^{(1)} - \boldsymbol{\mu}_i^{(-1)}$ and $\boldsymbol{\mu}^\star = \boldsymbol{\mu}^{\star(1)} - \boldsymbol{\mu}^{\star(-1)}$.

The Euclidean distance becomes:

$$\|\boldsymbol{\theta}_i - \boldsymbol{\theta}^\star\| = \sqrt{(\boldsymbol{\mu}_i - \boldsymbol{\mu}^\star)^\top \boldsymbol{\Sigma}^{-2} (\boldsymbol{\mu}_i - \boldsymbol{\mu}^\star)}.$$

For the total variation distance between the Gaussian distributions:

$$\mathrm{D}_{\mathrm{TV}}(D_i, D^\star) = \frac{1}{2}\|\boldsymbol{\mu}_i - \boldsymbol{\mu}^\star\|_{\boldsymbol{\Sigma}^{-1}} = \frac{1}{2}\sqrt{(\boldsymbol{\mu}_i - \boldsymbol{\mu}^\star)^\top \boldsymbol{\Sigma}^{-1} (\boldsymbol{\mu}_i - \boldsymbol{\mu}^\star)}.$$

Combining these, we derive the proportional relationship:

$$\|\boldsymbol{\theta}_i - \boldsymbol{\theta}^\star\| = C \cdot \mathrm{D}_{\mathrm{TV}}(D_i, D^\star),$$

where

$$C = 2\sqrt{\frac{(\boldsymbol{\mu}_i - \boldsymbol{\mu}^\star)^\top \boldsymbol{\Sigma}^{-2} (\boldsymbol{\mu}_i - \boldsymbol{\mu}^\star)}{(\boldsymbol{\mu}_i - \boldsymbol{\mu}^\star)^\top \boldsymbol{\Sigma}^{-1} (\boldsymbol{\mu}_i - \boldsymbol{\mu}^\star)}}.$$

To express this constant C further, we utilize the eigenvalue decomposition of the covariance matrix $\boldsymbol{\Sigma}$. Let:

$$\boldsymbol{\Sigma} = \mathbf{Q}\boldsymbol{\Lambda}\mathbf{Q}^\top,$$

where $\mathbf{Q}$ is the orthogonal matrix of eigenvectors of $\boldsymbol{\Sigma}$ and $\boldsymbol{\Lambda}$ is the diagonal matrix containing the eigenvalues $\lambda_1, \lambda_2, \ldots, \lambda_d$. Since $\boldsymbol{\Sigma}$ is positive definite, all eigenvalues $\lambda_j > 0$.

We rewrite the mean difference $\boldsymbol{\mu}_i - \boldsymbol{\mu}^\star$ in the eigenvector basis:

$$\tilde{\boldsymbol{\mu}} = \mathbf{Q}^\top (\boldsymbol{\mu}_i - \boldsymbol{\mu}^\star).$$

Here, $\tilde{\boldsymbol{\mu}}$ represents the coordinates of the mean difference in the space spanned by the eigenvectors of $\boldsymbol{\Sigma}$, and $\tilde{\mu}_j$ are its components.

The inverse and squared inverse of $\boldsymbol{\Sigma}$ are:

$$\boldsymbol{\Sigma}^{-1} = \mathbf{Q}\boldsymbol{\Lambda}^{-1}\mathbf{Q}^\top, \quad \boldsymbol{\Sigma}^{-2} = \mathbf{Q}\boldsymbol{\Lambda}^{-2}\mathbf{Q}^\top.$$

Substituting these into the expression for C, we get:

$$C = 2\sqrt{\frac{\tilde{\boldsymbol{\mu}}^\top \boldsymbol{\Lambda}^{-2} \tilde{\boldsymbol{\mu}}}{\tilde{\boldsymbol{\mu}}^\top \boldsymbol{\Lambda}^{-1} \tilde{\boldsymbol{\mu}}}}.$$

Writing out the components explicitly:

$$C = 2\sqrt{\frac{\sum_{j=1}^d \frac{\tilde{\mu}_j^2}{\lambda_j^2}}{\sum_{j=1}^d \frac{\tilde{\mu}_j^2}{\lambda_j}}}.$$

This final form shows that the proportionality constant C depends on the eigenvalues of the covariance matrix $\boldsymbol{\Sigma}$ and the components $\tilde{\mu}_j$ of the transformed mean difference. It encapsulates how the mean differences project onto the eigenvectors of the covariance matrix. □

Step 3: Formulating the Quadratic Optimization Problem Our objective is to determine the optimal combination coefficients $\gamma_i^\star$ that minimize the squared distance between the combined parameters $\boldsymbol{\theta}^{\mathrm{P}}$ and the target parameter $\boldsymbol{\theta}^\star$:

$$\min_\gamma \left\|\boldsymbol{\theta}^{\mathrm{P}} - \boldsymbol{\theta}^\star\right\|^2 = \min_\gamma \left\|\sum_{i=1}^n \gamma_i^\star \tilde{\boldsymbol{\theta}}_i - \boldsymbol{\theta}^\star\right\|^2,$$

subject to the constraints:

$$\sum_{i=1}^n \gamma_i^\star = 1, \quad \gamma_i^\star \geq 0.$$

Let $\boldsymbol{\delta}_i = \tilde{\boldsymbol{\theta}}_i - \boldsymbol{\theta}^\star$. Then, the objective function becomes:

$$\left\|\boldsymbol{\theta}^{\mathrm{P}} - \boldsymbol{\theta}^\star\right\|^2 = \left\|\sum_{i=1}^n \gamma_i^\star \boldsymbol{\delta}_i\right\|^2 = \sum_{i=1}^n \sum_{j=1}^n \gamma_i^\star \gamma_j^\star \boldsymbol{\delta}_i^\top \boldsymbol{\delta}_j.$$

Using the proportional relationship from Lemma 2, we express the inner product $\boldsymbol{\delta}_i^\top \boldsymbol{\delta}_j$ as:

$$\boldsymbol{\delta}_i^\top \boldsymbol{\delta}_j = \frac{1}{2}\left(\|\boldsymbol{\delta}_i\|^2 + \|\boldsymbol{\delta}_j\|^2 - \|\boldsymbol{\delta}_i - \boldsymbol{\delta}_j\|^2\right) = \frac{C^2}{2}\left(\mathrm{D}_{\mathrm{TV}}(D_i, D^\star)^2 + \mathrm{D}_{\mathrm{TV}}(D_j, D^\star)^2 - \mathrm{D}_{\mathrm{TV}}(D_i, D_j)^2\right),$$

where C is a positive constant of proportionality.

Define the symmetric matrix $\mathbf{H}$ with elements:

$$H_{ij} = \mathrm{D}_{\mathrm{TV}}(D_i, D^\star)^2 + \mathrm{D}_{\mathrm{TV}}(D_j, D^\star)^2 - \mathrm{D}_{\mathrm{TV}}(D_i, D_j)^2.$$

Thus, the objective function simplifies to:

$$\left\| \boldsymbol{\theta}^{\mathrm{P}} - \boldsymbol{\theta}^\star \right\|^2 = \frac{C^2}{2} \boldsymbol{\gamma}^{*\top} \mathbf{H} \boldsymbol{\gamma}^\star.$$

Since $\frac{C^2}{2}$ is a positive constant, minimizing $\left\| \boldsymbol{\theta}^{\mathrm{P}} - \boldsymbol{\theta}^\star \right\|^2$ is equivalent to minimizing $\boldsymbol{\gamma}^{*\top} \mathbf{H} \boldsymbol{\gamma}^\star$. Therefore, the optimization problem becomes:

$$\min_{\boldsymbol{\gamma}^\star} \boldsymbol{\gamma}^{*\top} \mathbf{H} \boldsymbol{\gamma}^\star, \quad \text{subject to} \quad \sum_{i=1}^{n} \gamma_i^\star = 1, \quad \gamma_i^\star \geq 0.$$

Step 4: Solving the Quadratic Optimization Problem We need to discuss by cases:

Case 1: $n = 2$

For $n = 2$, let $\gamma_2^\star = 1 - \gamma_1^\star$. Substituting into the objective function:

$$\boldsymbol{\gamma}^{*\top} \mathbf{H} \boldsymbol{\gamma}^\star = H_{11}(\gamma_1^\star)^2 + 2H_{12}\gamma_1^\star(1 - \gamma_1^\star) + H_{22}(1 - \gamma_1^\star)^2.$$

Expanding and simplifying:

$$\boldsymbol{\gamma}^{*\top} \mathbf{H} \boldsymbol{\gamma}^\star = (H_{11} + H_{22} - 2H_{12})(\gamma_1^\star)^2 + 2(H_{12} - H_{22})\gamma_1^\star + H_{22}.$$

To find the minimum, take the derivative with respect to $\gamma_1^\star$ and set it to zero:

$$\frac{d}{d\gamma_1^\star}(\boldsymbol{\gamma}^{*\top} \mathbf{H} \boldsymbol{\gamma}^\star) = 2(H_{11} + H_{22} - 2H_{12})\gamma_1^\star + 2(H_{12} - H_{22}) = 0.$$

Solving for $\gamma_1^\star$:

$$\gamma_1^\star = \frac{H_{22} - H_{12}}{H_{11} + H_{22} - 2H_{12}} = \frac{\mathrm{D}_{\mathrm{TV}}(D_2, D^\star)^2 + \mathrm{D}_{\mathrm{TV}}(D_1, D_2)^2 - \mathrm{D}_{\mathrm{TV}}(D_1, D^\star)^2}{2\mathrm{D}_{\mathrm{TV}}(D_1, D_2)^2}.$$

Thus, the optimal coefficients are:

$$\gamma_1^\star = \frac{\mathrm{D}_{\mathrm{TV}}(D_2, D^\star)^2 + \mathrm{D}_{\mathrm{TV}}(D_1, D_2)^2 - \mathrm{D}_{\mathrm{TV}}(D_1, D^\star)^2}{2\mathrm{D}_{\mathrm{TV}}(D_1, D_2)^2}, \quad \gamma_2^\star = 1 - \gamma_1^\star.$$

This solution is valid provided that $\gamma_1^\star, \gamma_2^\star \geq 0$.

Case 2: $n > 2$

When $n > 2$, an explicit solution for the optimal combination coefficients $\boldsymbol{\gamma}^\star$ generally does not exist under the constraints $\gamma_i^\star \geq 0$ due to the complexity introduced by multiple inequality constraints. However, if we further assume that all $\gamma_i^\star > 0$, we can derive an explicit solution.

Under the assumption $\gamma_i^\star > 0$ for all i, the optimization problem can be solved using the method of Lagrange multipliers. Construct the Lagrangian:

$$\mathcal{L}(\boldsymbol{\gamma}^\star, \lambda) = \boldsymbol{\gamma}^{*\top} \mathbf{H} \boldsymbol{\gamma}^\star - \lambda \left(\sum_{i=1}^{n} \gamma_i^\star - 1 \right).$$

Taking the derivative with respect to $\boldsymbol{\gamma}^\star$ and setting it to zero:

$$2\mathbf{H}\boldsymbol{\gamma}^\star - \lambda \mathbf{e} = 0 \quad \Rightarrow \quad \boldsymbol{\gamma}^\star = \frac{\lambda}{2} \mathbf{H}^{-1} \mathbf{e},$$

where $\mathbf{e}$ is an n-dimensional vector of ones.

Applying the constraint $\sum_{i=1}^{n} \gamma_i^\star = 1$:

$$\mathbf{e}^\top \boldsymbol{\gamma}^\star = \frac{\lambda}{2}\mathbf{e}^\top \mathbf{H}^{-1}\mathbf{e} = 1 \quad \Rightarrow \quad \lambda = \frac{2}{\mathbf{e}^\top \mathbf{H}^{-1}\mathbf{e}}.$$

Substituting back, the optimal combination coefficients are:

$$\boldsymbol{\gamma}^\star = \frac{\mathbf{H}^{-1}\mathbf{e}}{\mathbf{e}^\top \mathbf{H}^{-1}\mathbf{e}}.$$

This explicit solution holds provided that the matrix $\mathbf{H}$ is invertible and all resulting $\gamma_i^\star > 0$. If any $\gamma_i^\star \leq 0$, then numerical optimization methods must be employed to determine the optimal coefficients.

□

F Detailed Explanation of Parameter Transformation

In this appendix, we provide a comprehensive theoretical exposition of the parameter transformation techniques introduced in Section 4.1.

F.1 Learnable Width Transformation

The width transformation is designed to adapt the weight matrices from a pre-trained source model to match the input and output dimensions of a target model, which may differ due to architectural changes. Given a weight matrix $\boldsymbol{\theta} \in \mathbb{R}^{d_{\text{in}} \times d_{\text{out}}}$ from a layer of the source model, our goal is to compute a transformed weight matrix $\tilde{\boldsymbol{\theta}} \in \mathbb{R}^{d'_{\text{in}} \times d'_{\text{out}}}$ suitable for the corresponding layer in the target model.

To facilitate this transformation, we introduce learnable transformation matrices $\mathbf{c}_{\text{in}} \in \mathbb{R}^{d'_{\text{in}} \times d_{\text{in}}}$ and $\mathbf{c}_{\text{out}} \in \mathbb{R}^{d'_{\text{out}} \times d_{\text{out}}}$. These matrices map the source input and output dimensions to the target dimensions, respectively. The transformed weight matrix is computed as:

$$\tilde{\boldsymbol{\theta}} = \mathbf{c}_{\text{in}} \boldsymbol{\theta} \mathbf{c}_{\text{out}}^\top.$$

The matrices $\mathbf{c}_{\text{in}}$ and $\mathbf{c}_{\text{out}}$ are treated as learnable parameters, optimized to minimize the loss function $\mathcal{L}$ of the target model. To provide a meaningful initialization that captures the most significant components of $\boldsymbol{\theta}$, we employ Singular Value Decomposition (SVD) on $\boldsymbol{\theta}$. Specifically, we decompose $\boldsymbol{\theta}$ as:

$$\boldsymbol{\theta} = \mathbf{U}\boldsymbol{\Sigma}\mathbf{V}^\top,$$

where: - $\mathbf{U} \in \mathbb{R}^{d_{\text{in}} \times r}$ contains the left singular vectors, - $\boldsymbol{\Sigma} \in \mathbb{R}^{r \times r}$ is a diagonal matrix of singular values, - $\mathbf{V} \in \mathbb{R}^{d_{\text{out}} \times r}$ contains the right singular vectors, - $r = \text{rank}(\boldsymbol{\theta})$.

To align the dimensions with the target model, we truncate or extend $\mathbf{U}$ and $\mathbf{V}$ to obtain $\tilde{\mathbf{U}} \in \mathbb{R}^{d_{\text{in}} \times r'}$ and $\tilde{\mathbf{V}} \in \mathbb{R}^{d_{\text{out}} \times r'}$, where $r' = \min(d'_{\text{in}}, d'_{\text{out}}, r)$. The truncated singular values are $\tilde{\boldsymbol{\Sigma}} \in \mathbb{R}^{r' \times r'}$. Formally:

$$\tilde{\mathbf{U}} = \mathbf{U}_{[:,1:r']}, \tilde{\boldsymbol{\Sigma}} = \boldsymbol{\Sigma}_{[1:r',1:r']}, \tilde{\mathbf{V}} = \mathbf{V}_{[:,1:r']}.$$

We initialize the transformation matrices $\mathbf{c}_{\text{in}}$ and $\mathbf{c}_{\text{out}}$ based on the truncated SVD components:

$$\mathbf{c}_{\text{in}}^{(0)} = \mathbf{W}_{\text{in}} \tilde{\mathbf{U}}^\top, \mathbf{c}_{\text{out}}^{(0)} = \mathbf{W}_{\text{out}} \tilde{\mathbf{V}}^\top,$$

where $\mathbf{W}_{\text{in}} \in \mathbb{R}^{d'_{\text{in}} \times r'}$ and $\mathbf{W}_{\text{out}} \in \mathbb{R}^{d'_{\text{out}} \times r'}$ are learnable weight matrices initialized randomly or based on heuristics.

Substituting and the transformed weight matrix becomes:

$$\tilde{\boldsymbol{\theta}} = \mathbf{W}_{\text{in}}\tilde{\mathbf{U}}^{\top}\boldsymbol{\theta}\tilde{\mathbf{V}}\mathbf{W}_{\text{out}}^{\top}.$$

Using the properties of SVD, we have:

$$\tilde{\mathbf{U}}^{\top}\boldsymbol{\theta}\tilde{\mathbf{V}} = \tilde{\mathbf{U}}^{\top}(\mathbf{U}\boldsymbol{\Sigma}\mathbf{V}^{\top})\tilde{\mathbf{V}} = (\tilde{\mathbf{U}}^{\top}\mathbf{U})\boldsymbol{\Sigma}(\mathbf{V}^{\top}\tilde{\mathbf{V}}) = \mathbf{I}_{r'}\tilde{\boldsymbol{\Sigma}}\mathbf{I}_{r'}^{\top} = \tilde{\boldsymbol{\Sigma}},$$

where $\mathbf{I}_{r'}$ is the identity matrix of size $r' \times r'$. Hence, the transformed weight matrix simplifies to:

$$\tilde{\boldsymbol{\theta}} = \mathbf{W}_{\text{in}}\tilde{\boldsymbol{\Sigma}}\mathbf{W}_{\text{out}}^{\top}.$$

This formulation decouples the adaptation process into learning $\mathbf{W}_{\text{in}}$ and $\mathbf{W}_{\text{out}}$, which project the truncated singular values to the target dimensions. Both $\mathbf{W}_{\text{in}}$ and $\mathbf{W}_{\text{out}}$ are learnable parameters optimized during training.

During training, the transformation matrices $\mathbf{c}_{\text{in}}$ and $\mathbf{c}_{\text{out}}$ are updated to minimize the loss function $\mathcal{L}$. The gradients with respect to these matrices are computed via backpropagation. For $\mathbf{c}_{\text{in}}$, the gradient is:

$$\frac{\partial \mathcal{L}}{\partial \mathbf{c}_{\text{in}}} = \frac{\partial \mathcal{L}}{\partial \tilde{\boldsymbol{\theta}}}\frac{\partial \tilde{\boldsymbol{\theta}}}{\partial \mathbf{c}_{\text{in}}},$$

where:

$$\frac{\partial \tilde{\boldsymbol{\theta}}}{\partial \mathbf{c}_{\text{in}}} = \boldsymbol{\theta}\mathbf{c}_{\text{out}}^{\top}.$$

Similarly, for $\mathbf{c}_{\text{out}}$:

$$\frac{\partial \mathcal{L}}{\partial \mathbf{c}_{\text{out}}} = \frac{\partial \mathcal{L}}{\partial \tilde{\boldsymbol{\theta}}}\frac{\partial \tilde{\boldsymbol{\theta}}}{\partial \mathbf{c}_{\text{out}}},$$

with:

$$\frac{\partial \tilde{\boldsymbol{\theta}}}{\partial \mathbf{c}_{\text{out}}} = (\mathbf{c}_{\text{in}}\boldsymbol{\theta})^{\top}.$$

Using these gradients, the transformation matrices are updated as:

$$\mathbf{c}_{\text{in}} \leftarrow \mathbf{c}_{\text{in}} - \eta\frac{\partial \mathcal{L}}{\partial \mathbf{c}_{\text{in}}}, \mathbf{c}_{\text{out}} \leftarrow \mathbf{c}_{\text{out}} - \eta\frac{\partial \mathcal{L}}{\partial \mathbf{c}_{\text{out}}},$$

where η is the learning rate.

F.2 Learnable Depth Transformation

The depth transformation adjusts the number of layers from L in the source model to L' in the target model. We introduce a learnable depth transformation matrix $\mathbf{D}_{\text{depth}} \in \mathbb{R}^{L' \times L}$, where each element d_{ki} represents the learnable contribution of the i-th source layer to the k-th target layer.

The transformed parameters for the k-th target layer are computed as:

$$\tilde{\boldsymbol{\theta}}^{k} = \sum_{i=1}^{L} d_{ki}\boldsymbol{\theta}^{i},$$

with the constraints:

$$d_{ki} \geq 0, \quad \sum_{i=1}^{L} d_{ki} = 1 \quad \forall k.$$

To satisfy the constraints, we parameterize d_{ki} using the softmax function over learnable logits γ_{ki}:

$$d_{ki} = \frac{\exp(\gamma_{ki})}{\sum_{j=1}^{L} \exp(\gamma_{kj})}.$$

This formulation ensures that d_{ki} are positive and sum to one for each k.

The logits γ_{ki} are optimized alongside the model parameters by minimizing the overall loss $\mathcal{L}$. The gradient updates are:

$$\gamma_{ki} \leftarrow \gamma_{ki} - \eta \frac{\partial \mathcal{L}}{\partial \gamma_{ki}}.$$

The learnable coefficients d_{ki} allow the model to dynamically determine the importance of each source layer for constructing the target layers.

G Additional Related Work

Knowledge distillation (KD) (Hinton et al., 2015) is a widely used technique for transferring knowledge from a larger teacher model to a smaller student model by training the student to mimic the teacher's output logits or representations. The primary focus of KD is on transferring knowledge through the output space, aiming for model compression and efficiency without significant loss in performance.

Various extensions of KD have been proposed to improve efficiency and performance. Self-distillation (Zhang et al., 2019) involves training a model using its own outputs as soft targets, while mutual learning (Zhang et al., 2018) involves co-training multiple models to learn from each other. In the context of large-scale models, KD has been applied to compress transformer-based architectures (Sanh et al., 2019; Jiao et al., 2019) and to improve model generalization (Yuan et al., 2020).

Recent advances in KD have explored more sophisticated approaches. Cross-modal knowledge distillation (Gou et al., 2021) enables knowledge transfer between models operating on different modalities. Contrastive knowledge distillation (Tian et al., 2020) leverages contrastive learning to capture fine-grained structural knowledge. Additionally, adaptive knowledge distillation (Song et al., 2022) dynamically adjusts the distillation process based on the learning status of the student model.

While KD focuses on output-space knowledge transfer, our proposed method, SAIL, operates at the parameter level. SAIL directly transforms and integrates parameters from multiple pre-trained models to initialize a new model, leveraging the collective knowledge embedded in their parameters. This approach differs from KD in that it does not require training a student model to mimic a teacher's outputs; instead, it constructs a proximal parameter initialization that accelerates convergence during training.

Moreover, SAIL can be considered complementary to knowledge distillation. After applying SAIL to initialize the target model, KD can be employed as a subsequent optimization step to fine-tune or align the model to specific tasks. This combination could enhance both training efficiency and model performance by leveraging both parameter-space and output-space knowledge transfer.

H EXPERIMENTAL DETAILS

H.1 DATA DESCRIPTION

Our experiments primarily used the OpenWebText dataset, a large-scale corpus of web content. For cross-dataset generalization experiments, we also utilized the WikiText-103 dataset. Additionally, we conducted computer vision experiments using CIFAR-10, CIFAR-100, and Tiny ImageNet datasets.

OpenWebText: This dataset consists of web content extracted from URLs shared on Reddit. It contains a diverse range of topics and writing styles, making it suitable for training general-purpose language models. The dataset is stored in a binary format (‘train.bin‘) where each token is represented as a 16-bit integer. Our preprocessed version of OpenWebText contains approximately 9 billion tokens.

WikiText-103: This dataset is derived from the set of verified Good and Featured articles on Wikipedia. It contains over 100 million tokens and serves as a high-quality benchmark for language modeling tasks. WikiText-103 is known for its long-term dependencies and diverse vocabulary, making it an excellent test for model generalization.

Data Preprocessing for NLP Tasks: For our experiments, we split the OpenWebText dataset into three subsets (D1, D2, and Dt) based on the mean token value of data blocks. This feature-based splitting approach ensures that each subset has a distinct distribution, allowing us to simulate different data domains. The splitting process is as follows:

1. We compute the mean token value for each block of 1024 tokens in the dataset.
2. We sort these blocks based on their mean token values.
3. We use the 33rd and 66th percentiles of these mean values as thresholds to split the data into three parts:
   - D1: Blocks with mean token values below the 33rd percentile
   - D2: Blocks with mean token values between the 33rd and 66th percentiles
   - Dt: Blocks with mean token values above the 66th percentile

This approach ensures that each subset has a distinct statistical distribution, simulating different data domains while still being part of the same overall corpus.

T-SNE Visualizations: To verify the effectiveness of our splitting approach and to visualize the distributions of different datasets, we performed more t-SNE (t-Distributed Stochastic Neighbor Embedding) analysis. Figure 4 presents a t-SNE visualization comparing samples from OpenWebText and WikiText-103, illustrating the distributional differences between these datasets.

Computer Vision Datasets: For our computer vision experiments, we used the following datasets:

- **CIFAR-10:** A dataset of 60,000 32x32 color images in 10 classes, with 6,000 images per class. There are 50,000 training images and 10,000 test images.
- **CIFAR-100:** Similar to CIFAR-10, but with 100 classes containing 600 images each. There are 500 training images and 100 testing images per class.
- **Tiny ImageNet:** A subset of ImageNet, consisting of 200 classes with 500 training images, 50 validation images, and 50 test images per class. Each image is 64x64 pixels.

These datasets were chosen to evaluate our method’s performance across different levels of task complexity and dataset sizes in the computer vision domain.

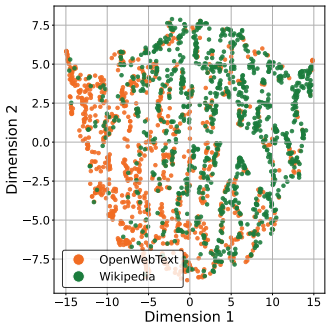

Figure 4: t-SNE visualization comparing OpenWebText and WikiText-103 samples

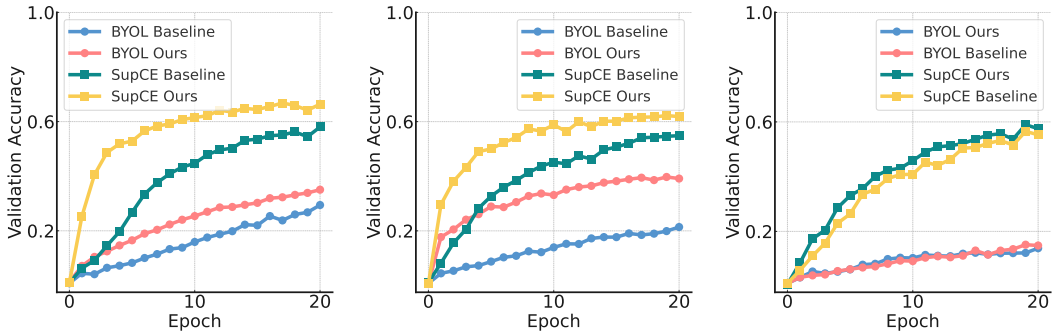

(a) ResNet-18 Modified (CIFAR-100) (b) Standard ResNet-18 (CIFAR-100) (c) ResNet-34 Modified (CIFAR-100)

Figure 5: **Accuracy in Different ResNet Configurations: (a)** Accuracy of ResNet-18 Modified trained with BYOL and SupCE on CIFAR-100. **(b)** Accuracy of standard ResNet-18 trained with BYOL and SupCE on CIFAR-100. **(c)** Accuracy of ResNet-34 Modified trained with BYOL and SupCE on CIFAR-100.

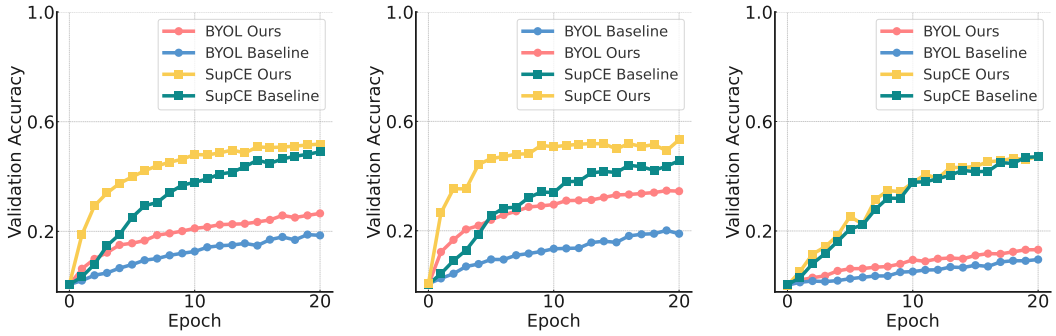

(a) ResNet-18 Modified (Tiny-ImageNet) (b) Standard ResNet-18 (Tiny-ImageNet) (c) ResNet-34 Modified (Tiny-ImageNet)

Figure 6: **Accuracy in Different ResNet Configurations: (a)** Accuracy of ResNet-18 Modified trained with BYOL and SupCE on Tiny-ImageNet. **(b)** Accuracy of standard ResNet-18 trained with BYOL and SupCE on Tiny-ImageNet. **(c)** Accuracy of ResNet-34 Modified trained with BYOL and SupCE on Tiny-ImageNet.

Detailed results for CIFAR-100 and Tiny ImageNet experiments are presented in Section H.2 of this appendix.

H.2 Additional Experimental Results

I Experiments in NLP

In this section, we present a comprehensive evaluation of our proposed method, **Sail**, in comparison with various baseline methods across multiple natural language processing (NLP) benchmarks. Leveraging the fully open **OLMo** framework, which includes model weights, training data, and evaluation tools, we ensure reproducibility and transparency in our experimental setup. We detail our experimental setup, including model configurations derived from the OLMo-1B and OLMo-7B variants, training procedures informed by our custom configuration file, hyperparameters, and dataset specifics. The results demonstrate the efficacy of **Sail** in enhancing model performance through optimal parameter merging and initialization.

I.1 Experimental Setup

I.1.1 Models Used

We conducted our experiments using the following models from the OLMo Groeneveld et al. (2024):

OLMo-1B: A 1-billion parameter model pretrained on a diverse corpus, designed for general-purpose language understanding. **OLMo-7B**: A 7-billion parameter model with enhanced capabilities for complex language understanding and reasoning tasks. Each model variant is trained with distinct architectures, optimizers, and hardware configurations as specified in our training configuration file. The OLMo framework provides multiple checkpoints, enabling us to select intermediate states for parameter merging and initialization.

I.1.2 Checkpoint Selection

For constructing the parameter set using **Sail**, we selected intermediate checkpoints based on the training progress captured in the OLMo:

- **OLMo-1B**: Intermediate checkpoints at steps 500,000 (`steps500000-2097B`), 600,000 (`steps600000-2517B`), and 700,000 (`steps700000-2936B`) were selected. These checkpoints represent different stages of model convergence and training dynamics.
- **OLMo-7B**: A single intermediate checkpoint at step 474,000 (`steps474000-2097B`) was selected, providing a reference point for evaluating larger model performance.

I.1.3 Training Configuration

Table 1 outlines the hyperparameters employed for training with **Sail**. These settings were chosen based on preliminary experiments and best practices in the literature to optimize model performance.

Table 1: Hyperparameters for **Sail**

Hyperparameter	Value
Batch Size	16
Learning Rate	4e-4
Optimizer	AdamW
Number of Epochs	1
Weight Decay	0.01
Gradient Clipping	1.0
Scheduler	Cosine with Warmup
Warmup Steps	2000

I.2 Dataset Details

We evaluated our models on a diverse set of NLP benchmarks to ensure a comprehensive assessment of **Sail**'s capabilities. The datasets encompass a range of tasks, including commonsense reasoning, question answering, and causal reasoning. Below are the details of each dataset used:

- **PIQA**:Bisk et al. (2020) Physical commonsense reasoning with 7,000 training examples and 1,500 test examples.
- **HellaSwag**:Zellers et al. (2019) Complex multiple-choice questions requiring robust inference, consisting of 70,000 training examples and 10,000 test examples.
- **Winogrande**:ai2 (2019) Pronoun resolution with 44,000 training examples and 8,000 test examples.
- **SciQ**:Johannes Welbl (2017) Comprehension of scientific texts, containing 13,679 training examples and 1,384 test examples.
- **ARC-Easy**:Clark et al. (2018) Grade-school level science questions with 3,779 training examples and 1,366 test examples.
- **COPA**:Roemmele et al. (2011) Causal reasoning by selecting plausible alternatives, comprising 1,000 training examples and 500 test examples.

I.3 COMPLETE RESULTS

We present a comprehensive comparison of **Sail** against various baseline methods across all evaluated NLP benchmarks. The results are consolidated in Table 2, demonstrating the superior performance and flexibility of **Sail** in model initialization and parameter merging.

Table 2: Comparison of **Sail** with Baseline Methods (Accuracy %)

Dataset	Train from Scratch	LIGO	Uniform Soup	Greedy Soup	Sail (Ours)
PIQA	51.96	52.29	54.80	57.73	**61.92**
HellaSwag	24.87	25.33	25.25	27.65	**34.48**
Winogrande	51.14	50.20	50.51	52.09	**52.96**
SciQ	22.10	23.90	51.90	59.70	**70.30**
ARC-Easy	27.54	29.65	27.19	34.91	**42.63**
COPA	58.00	55.00	57.00	51.00	**63.00**

Comparison of Sail with Baseline Methods These curves display perplexity across step for models initialized with **Sail** compared to those with random initialization. The plots confirm that **Sail** not only achieves higher final performance but also converges more rapidly during training, consistent with our findings in computer vision (CV) experiments.

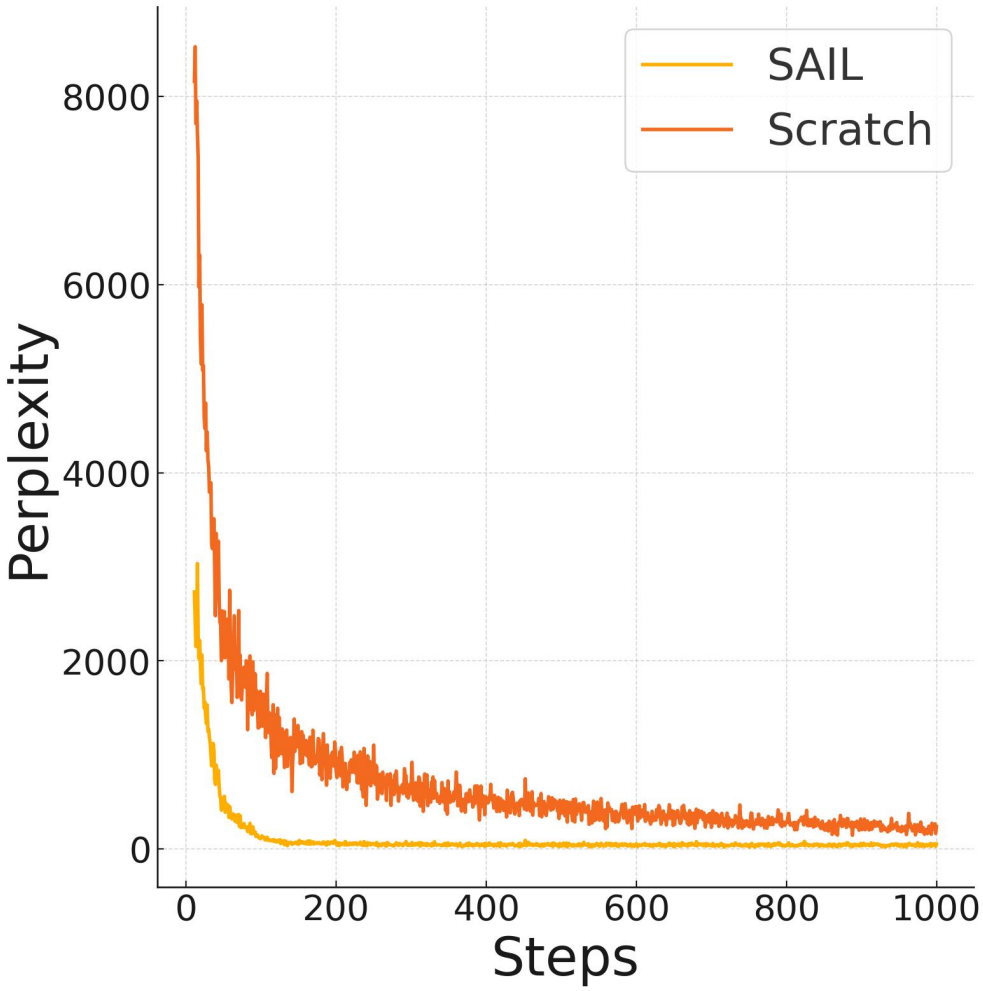

Figure 7: Perplexity for Models Initialized with **Sail** vs. Random Initialization on NLP Benchmarks.

J SAIL FOR SiT DIFFUSION MODELS

J.1 APPLYING SAIL TO SiT DIFFUSION MODELS

In this section, we extend our Structured-Initialization Learning (SAIL) framework to accelerate the training of state-of-the-art SiT (Scalable Interpolant Transformers) diffusion models (Ma et al., 2024), which are generative models. By adapting SAIL to SiT diffusion models, we aim to demonstrate the versatility of our method in different domains and its effectiveness in improving training efficiency.

In visual representation learning, aligning the representations within generative models with pre-trained ones improves both semantic integration and performance (Yu et al., 2024). Within our SAIL framework, this alignment is achieved through specific adaptations. One such adaptation is Latent-to-Representation alignment, which serves as a case study for applying SAIL to SiT models, given that SiT training occurs in latent space of VAE (Ma et al., 2024).

Formally, let us denote:

- $\mathcal{Z}$ as the latent space of the diffusion model.
- $\mathcal{R}$ as the external pre-trained representation space.
- $f_{\mathrm{P}} : \mathcal{Z} \to \mathcal{R}$ as the pre-trained representation model.
- $f_{\mathrm{A}} : \mathcal{H} \to \mathcal{R}$ as the alignment function within SAIL, where $\mathcal{H}$ represents the hidden representations of the diffusion model.

The objective is to minimize the discrepancy between the representations derived from the VAE latent space and those from the pre-trained representation space, ensuring coherent semantic alignment within the SAIL framework.

J.2 WEIGHT INITIALIZATION IN SAIL FOR SiT MODELS

Using SAIL, we initialize the weights of the SiT diffusion transformer by leveraging pre-trained models. This corresponds to our parameter transformation technique, where we adjust the dimensions of pre-trained model parameters to match the target SiT architecture.

Formally, let $\boldsymbol{\theta}^{\mathrm{P}}_{\mathrm{SAIL}}$ represent the pre-trained weights obtained by optimizing the alignment between latent variables and pre-trained representations:

$$\boldsymbol{\theta}^{\mathrm{P}}_{\mathrm{SAIL}} = \arg\min_{\boldsymbol{\theta}} \mathcal{L}_{\mathrm{Align}}(\boldsymbol{\theta}), \tag{14}$$

where $\mathcal{L}_{\mathrm{Align}}$ is the alignment loss function within the SAIL framework that measures the discrepancy between the model's latent representations and the pre-trained representation space. By initializing the SiT model with $\boldsymbol{\theta}^{\mathrm{P}}_{\mathrm{SAIL}}$, we ensure that the model starts with parameters that already encode meaningful semantic information, thereby enhancing the efficiency of subsequent training stages.

J.3 INCORPORATING ALIGNMENT LOSS IN SAIL TRAINING

In addition to weight initialization, we incorporate an alignment loss term into the SAIL training objective to continuously align the model's hidden representations with the pre-trained representations. This strategy complements our proximal parameter integration and retraining approach, which efficiently combines transformed parameters to initialize new models.

The total loss function during training becomes:

$$\mathcal{L}_{\mathrm{Total}} = \mathcal{L}_{\mathrm{Velocity}} + \lambda_{\mathrm{REPA}}\mathcal{L}_{\mathrm{REPA}} + \lambda_{\mathrm{Align}}\mathcal{L}_{\mathrm{Align}}, \tag{15}$$

where:

- $\mathcal{L}_{\mathrm{Velocity}}$ is the primary loss for velocity prediction in the diffusion model.
- $\mathcal{L}_{\mathrm{REPA}}$ is the representation alignment loss as defined in REPA (Yu et al., 2024).

- $\mathcal{L}_{\text{Align}}$ is the alignment loss within SAIL.
- λ_{REPA} and λ_{Align} are hyperparameters controlling the strength of each alignment component.

The alignment loss is defined as:

$$\mathcal{L}_{\text{Align}} = \mathbb{E}_{\mathbf{z}_t, \mathbf{h}_t} \left[\| f_{\text{P}}(\mathbf{z}_t) - f_{\text{A}}(\mathbf{h}_t) \|^2 \right], \tag{16}$$

where:

- $\mathbf{z}_t$ represents the latent variables at time t.
- $\mathbf{h}_t$ represents the hidden states of the model at time t.

J.4 Experimental Setup

To evaluate the effectiveness of integrating Latent-to-Representation (L2R) alignment within the SAIL framework for improving SiT pre-training, we conduct a series of experiments on the ImageNet 256×256 dataset. Our primary objective is to assess how the incorporation of L2R influences both the training efficiency and the quality of the generated representations.

We utilize the ImageNet dataset, specifically the 256×256 resolution subset, which contains 1.28 million training images and 50,000 validation images across 1,000 classes. All images are resized to 256×256 pixels and normalized using standard ImageNet statistics. Data augmentation techniques, including random horizontal flipping and random cropping, are employed to enhance the diversity of the training data.

The SiT-B/2 model, as described by Ma et al. (2024), serves as our baseline architecture. We enhance the training of this model by integrating our SAIL outlined in the previous sections. Specifically, the L2R model was initialized with pre-trained weights obtained from an alignment task between latent variables and pre-trained representations, ensuring that the initial parameters encoded meaningful semantic information.

J.4.1 Hyperparameters

Following previous studies (Ma et al., 2024; Yu et al., 2024), the key hyperparameters for our experiments are summarized in Table 3.

Table 3: Hyperparameters used for training SAIL with L2R model on ImageNet 256×256.

Hyperparameter	**Value**
Learning Rate	1×10^{-4}
Optimizer	AdamW
β_1	0.9
β_2	0.999
Weight Decay	0.01
Batch Size	256
Training Iterations	400K
Gradient Clipping Norm	1.0
λ_{REPA}	0.5
λ_{L2R}	0.5
Latent Scale	0.18215
Latent Bias	0.0

J.5 Results

The integration of our SAIL framework significantly improve both the training efficiency and effectiveness of SiT. Table 4 provides a comparative analysis between the baseline SiT model and the enhanced version incorporating REPA and SAIL across various training iterations.

Table 4: Performance comparison between the baseline SiT model and the SiT model enhanced with REPA and SAIL at various training iterations over ImageNet 256×256 generation. Improvements with SAIL over REPA are indicated with arrows and highlighted in red.

Model	#Params	Iter.	FID↓	sFID↓	IS↑	Prec.↑
SiT-B/2 (Ma et al., 2024)	130M	400K	33.0	6.46	43.7	0.53
+ REPA	130M	50K	78.2	11.71	17.1	0.33
+ SAIL (ours)	130M	50K	67.6 (↓10.6)	16.19 (↑4.48)	20.5 (↑3.4)	0.34 (↑0.01)
+ REPA	130M	100K	49.5	7.00	27.5	0.46
+ SAIL (ours)	130M	100K	35.9 (↓13.6)	7.02 (↓0.02)	45.1 (↑17.6)	0.53 (↑0.07)
+ REPA	130M	200K	33.2	6.68	43.7	0.54
+ SAIL (ours)	130M	200K	19.8 (↓13.4)	6.15 (↓0.53)	81.9 (↑38.2)	0.64 (↑0.10)
+ REPA	130M	400K	24.4	6.40	59.9	0.59
+ SAIL (ours)	130M	400K	12.2 (↓12.2)	5.90 (↓0.50)	119.4 (↑59.5)	0.70 (↑0.11)

K CONTROL EXPERIMENTS WITH THE SPIRALS DATASET

To empirically validate our theoretical findings and demonstrate the practical effectiveness of the SAIL method, we conduct control experiments using the Spirals dataset. By considering different model initializations and non-overlapping data distributions, we aim to verify that our theoretical predictions hold in practice when applied to multi-layer perceptrons (MLPs).

The Spirals dataset is a synthetic dataset where data points are arranged in two interleaving spirals, forming a challenging classification problem that requires models to learn complex, non-linear decision boundaries (Guyon & Elisseeff, 2003). This dataset is well-suited for assessing the capability of models to capture intricate patterns and for evaluating the effectiveness of initialization strategies in non-convex optimization landscapes.

We design our experiments to achieve two main objectives:

1. **Faster Optimization Speed**: Demonstrate that models initialized with the SAIL method converge faster than those with random initialization.
2. **Effectiveness of SAIL under Different Data Distributions**: Assess the impact of using pre-trained models trained on different, non-overlapping subsets of the Spirals dataset to evaluate the limitations of the SAIL method.

K.1 EXPERIMENTAL SETUP

We generate the Spirals dataset $\mathcal{D}^\star$ consisting of data points from two interleaving spirals, with each spiral representing a distinct class. To create different, non-overlapping data distributions, we derive two additional separate subsets from $\mathcal{D}^\star$:

- $\mathcal{D}_1$: Contains data points exclusively from the first spiral, comprising the first 40% of the training data.
- $\mathcal{D}_2$: Contains data points exclusively from the second spiral, comprising the next 40% of the training data.

We train two models separately on these non-overlapping subsets:

- θ_1: Trained on $\mathcal{D}_1$.
- θ_2: Trained on $\mathcal{D}_2$.

Using the SAIL method, we transform and merge the parameters of θ_1 and θ_2 to form the proximal parameter θ^{P}, which serves as the initialization for training the target model on the full dataset $\mathcal{D}^\star$.

We compare the performance of models initialized with θ^{P} against models with random initialization and models trained on $\mathcal{D}^\star$ from scratch. All models are trained using the same neural network architecture: a multi-layer perceptron (MLP) with one hidden layer of 50 neurons and ReLU activation functions. The learning rate is set to 5×10^{-3}, and models are trained using the Adam optimizer for 300 epochs.

We evaluate the models based on three metrics: training loss, accuracy, and gradient norm. The gradient norm provides insight into the stability and efficiency of the optimization process.

Faster Optimization Speed Figure 8 shows the training loss and accuracy over epochs for the models initialized with θ^{P} and with random initialization. The model initialized with θ^{P} converges to a lower loss significantly faster than the randomly initialized model. The accuracy of the model with SAIL initialization improves rapidly and reaches a higher final accuracy compared to the model with random initialization. This demonstrates that the SAIL initialization provides a better starting point in the parameter space, closer to the optimum, thus requiring fewer iterations to converge.

Gradient Norm Analysis Figure 9 presents the gradient norm over epochs. The SAIL-initialized model exhibits a smaller gradient norm earlier in training, indicating a more stable optimization process. This suggests that the model starts closer to a region with flatter loss landscape, facilitating more efficient convergence compared to the randomly initialized model.

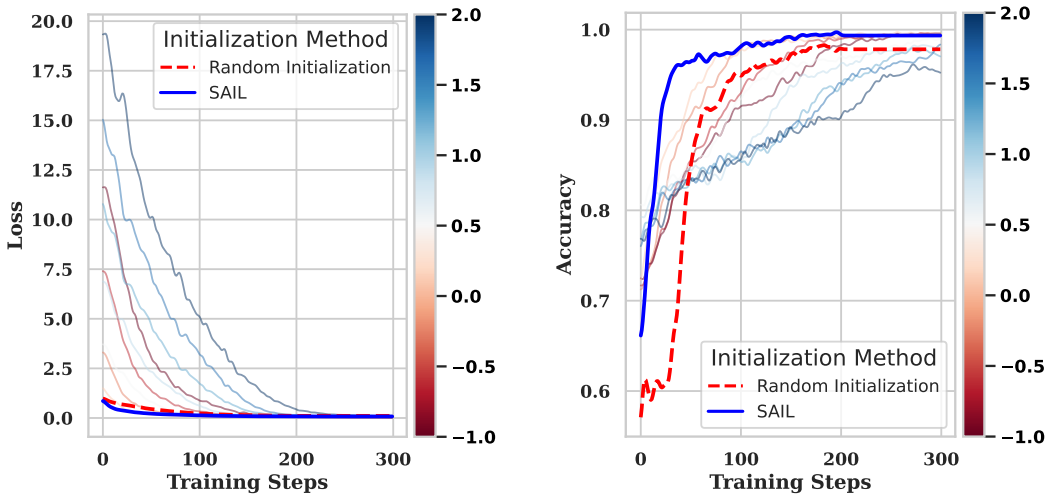

(a) Training Loss (b) Accuracy

Figure 8: Comparison of training loss and accuracy over epochs for models initialized with θ^{P} (SAIL) and with random initialization. The SAIL-initialized model converges faster and achieves better performance.

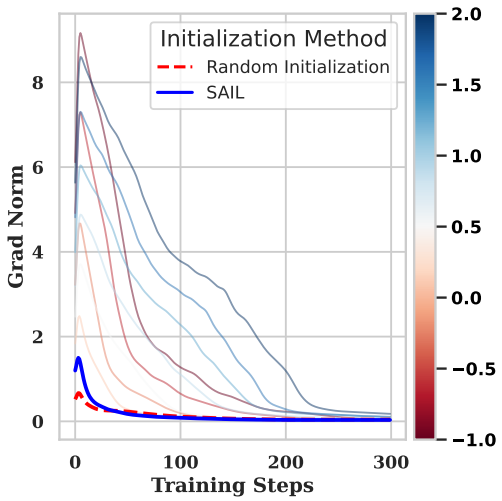

Figure 9: Gradient norm of the parameters over epochs for models initialized with θ^{P} (SAIL) and with random initialization. The SAIL-initialized model demonstrates a more stable optimization trajectory.

Effectiveness of SAIL under Different Data Distributions To assess the robustness of the SAIL method, we conducted experiments where the pre-trained models θ_1 and θ_2 were trained on different, non-overlapping subsets of $\mathcal{D}_1$ and $\mathcal{D}_2$. In this scenario, the benefits of the SAIL initialization are influenced by the disparity between the pre-trained models' data distributions and that of the target dataset $\mathcal{D}^\star$.

As shown in Figure 8 and Figure 9, even when the pre-trained models are trained on distinct and non-overlapping subsets, the SAIL initialization still provides a convergence speed advantage compared to random initialization, albeit reduced compared to the scenario where the pre-trained models are trained on larger or more representative portions of the target dataset.

These experiments confirm that the SAIL method effectively accelerates the convergence of MLP models on complex, non-convex tasks like the Spirals dataset. By initializing the model parameters with the proximal parameter θ^{P} derived from pre-trained models on related data, we achieve faster optimization and better final performance compared to random initialization. The method remains

effective even when the pre-trained models are trained on different, non-overlapping data distributions, demonstrating the versatility and robustness of SAIL.